IOP Publishing *Bioinspir. Biomim.* **00** (2014) 000000

Bioinspiration & Biomimetics

RECEIVED
6 March 2014

ACCEPTED FOR PUBLICATION
25 June 2014

PUBLISHED
DD MM 2014

SPECIAL ISSUES/SECTIONS

Multibody system dynamics for bio-inspired locomotion: from geometric structures to computational aspects

Frédéric Boyer[1] **and Mathieu Porez**[2]

[1] IRCCyN, Ecole des Mines de Nantes, La Chantrerie - 4, rue Alfred Kastler, B.P. 20722, 44307 NANTES Cedex 3, France
[2] IRCCyN, Ecole des Mines de Nantes, La Chantrerie - 4, rue Alfred Kastler, B.P. 20722, 44307 NANTES Cedex 3, France

E-mail: frederic.boyer@mines-nantes.fr **and** mathieu.porez@mines-nantes.fr

Keywords: biologically inspired robots, Lagrangian locomotion dynamics, geometric mechanics, multibody systems

Abstract

This article presents a set of generic tools for multibody system dynamics devoted to the study of bio-inspired locomotion in robotics. First, archetypal examples from the field of bio-inspired robot locomotion are presented to prepare the ground for further discussion. The general problem of locomotion is then stated. In considering this problem, we progressively draw a unified geometric picture of locomotion dynamics. For that purpose, we start from the model of discrete mobile multibody systems (MMSs) that we progressively extend to the case of continuous and finally soft systems. Beyond these theoretical aspects, we address the practical problem of the efficient computation of these models by proposing a Newton–Euler-based approach to efficient locomotion dynamics with a few illustrations of creeping, swimming, and flying.

1. Introduction

Compared with our robots, animals demonstrate dynamic performance, especially in terms of energy consumption and maneuverability, that we can only dream of [32]. Snakes have mastered every environment. They have several ways of crawling, can swim, and even glide through the air. And all that with an extremely simple geometry. Fish enjoy unrivaled underwater maneuverability and efficiency. They can reverse direction without even decelerating and swim in turbulent flows with little effort. Insects and hummingbirds are capable of extremely rapid and precise aerial maneuvers. Like fish, they have developed a very sophisticated strategy to recapture energy in their surrounding unsteady flow. As a result, there has been a great deal of interest over the last few decades in the design of locomotion robots inspired by animals. An emblematic example of these mechanisms is the snake-like robot ACM-III [43], a pioneering prototype that was a first milestone in bio-inspired terrestrial locomotion. Increasingly targeted robot performance and greater understanding of animal locomotion have since led to artificial locomotion systems adapted to broadly diverse surroundings, including unstructured terrains, water, and air.

As regards locomotion on unstructured terrain, snakes are a source of much inspiration for roboticists. The ACM-III was a two-meter wheeled multibody system with 21 segments serially connected by 20 actuated revolute joints each with a single degree of freedom. Its passive wheels reproduced the frictional anisotropy of ground friction forces, which in natural snakes is provided by the ventral scales present on their belly [37, 45]. Several wheel-less snake-like robots have since been developed for 2D or 3D locomotion in more unstructured environments [53, 82]. These highly articulated snake-like robots can perform more difficult tasks such as stair climbing, gap crossing, and channel climbing. In short, one of the key problems posed by this kind of system is to develop novel gaits capable of producing net displacement on difficult terrain [41].

In underwater robotics, when targeting maneuverability with high efficiency in open waters, the most advanced animal for bio-inspiration is probably the tuna fish, which can cruise up to 50 km h^{-1}. The red tuna can accelerate to up to 75 km h^{-1} and can reverse direction in a fraction of second. Seeking new solutions for drag reduction in naval hydrodynamics, Triantafyllou and co-workers were among the first to investigate the bio-inspired paradigm in this context [79]. In the RoboTuna project, several fish-like robots

inspired by the tuna were built at MIT in the 1990s. These robots consisted of a set of rigid vertebrae driven by an elaborate system of pulleys and cable tendons connected to servo motors mounted outside the robot body. After RoboTuna, another robotic fish was designed at MIT and named RoboPike. The aim of this new project was to reproduce the high accelerations of the pike (*Esox lucius*), which can reach 15 g (g = 9.81 ms^{-2}) when catching its prey. Unlike RoboTuna, this robot had its actuation mechanism inside its body. Following these projects, many swimming robots were then developed. Inspired by elongated anguilliform fishes such as the eel and the lamprey, some of them used undulation of the entire body with a high number of internal degrees of freedom instead of merely oscillating the rear part of their body (as did RoboTuna) to propel themselves in water [19]. Examples of such robots include the amphibious snake-like robots Amphibot [30], ACM-R5 [83], and the eel-like robot from the French project RAAMO [1].

Research into bio-inspired aerial robots has exploded in the last few years. These robots are commonly named micro aerial vehicles (MAVs). This nomenclature emerged in the late 1990s when the US defense agency DARPA defined them as aerial robots with a maximum dimension of 15 cm and a flight speed of 15–20 m s^{-1} [2]. Currently many successful prototypes and designs exist. Here we briefly review some of them. One of the pioneers in this field is R. J. Wood [81]. His first prototype weighed 60 mg and used piezoelectric actuators and insect-like passive wing pitching. It first flew in 2007, but it required a tether for power and stability. Another remarkable prototype is the DelFly ornithopter developed at the Technical University of Delft and Wageningen University [31], which is radio controlled using tail configurations resembling those of fixed-wing aircraft. Aerovironment's Nano Hummingbird [3], while not especially small, was a huge breakthrough in MAV research because of its gyroscopically stabilized flight without any tail surfaces. Hao Liu and co-workers at Chiba University [54] developed a hawk moth–inspired flapping-wing MAV, which is about 5 cm long, weighs less than 5 grams, and is capable of forward and hovering flight. A particularly interesting prototype was that developed by the Cornell Creative Machines Lab team [71]. With its 3D printed wings, this four-winged insect-like robot weighs 3.89 grams and has made an 85-second passively stable untethered hovering flight. In all these designs, the rigidity required for propulsion derives from the rigid components of the structures. However, inspired by hydrostats, which obtain the rigidity required for contact efficiency by contracting isovolume tissues, researchers are now designing soft body robots with no rigid components: octopus arms [4, 28] elephant's trunks [39], caterpillars [73], etc. Although the actuation of these systems remains a challenging task using current technologies, exploiting the passive deformations of soft organs to enhance locomotion has potential for the construction of a new generation of light, versatile robots. As such locomotion systems become more and more complex, so do their mathematical models. Thus, we now need efficient methodological tools to assist roboticists in modeling, design, control, motion planning (gait generation, transit maneuvers), etc. In this regard, dynamic models are of great interest to researchers due to their active role in simulation, design, and control. Bearing this growing interest in mind, one of the purposes of this article is to bring together the greatest possible number of existing locomotion cases in a unified, structured general picture complete with new applications for hyper-redundant continuous systems or soft robots with compliant organs. Remarkably, abstract tools of geometric mechanics introduced by Poincaré [66], Arnold [8], and Marsden [5] allow us to demonstrate the common geometric structures shared by apparently very different modes of locomotion and to classify them according to the basic properties of their Lagrangian dynamic model. To present these mathematical tools, we tried to leverage geometric intuition and physics insight as much as possible while maintaining the technical emphasis required by their practical application to real systems. In particular, this article also addresses the challenging issue of the computation of these models. Indeed, although the geometric Lagrangian picture is a powerful tool for analysis and classification, it is not suited for implementation in real complex systems as are the bio-inspired (hype-redundant, continuous, soft) systems currently developed in robotics labs. With this perspective, we present a unified synthetic picture of an alternative to the Lagrangian modeling based on the Newton–Euler formulation of multibody systems as developed to date for bio-inspired locomotion by the authors [13–15, 18, 50, 68]. This formulation makes it possible to derive efficient computational algorithms that are easy to implement. Here it is used to extend our investigations from discrete to continuous and finally to soft bio-inspired systems. The article is structured as follows. section 2 introduces some basic definitions used in the article. Then the general problem of locomotion addressed in the article is stated and discussed in section 3. It consists in computing forward locomotion dynamics controlled by internal d.o.f. as well as the inverse internal torque dynamics. The next two sections deal with forward locomotion dynamics in the kinematic case (section 4) and the dynamic case (section 5). Section 6 is devoted to the computation of torque dynamics. The practical implementation of these models through numerical algorithms is discussed in section 7. In all these developments, the constitutive bodies of the robots are considered as discrete, rigid bodies. The case of continuous systems is considered in section 8, which is followed by the case of soft systems (section 9) and a conclusion.

2. Basic definitions

In its essence, locomotion is based on the following principle. Any animal moving in space first changes its shape in order to exert some force on its surroundings. By virtue of the action-reaction principle, i.e., Newton's third law of motion, the surroundings exert reaction forces on the animal's body, which propel it in space. In the following, we adopt the model of multibody systems to derive a general unified framework devoted to the modeling of locomotion—and in particular bio-inspired locomotion—in robotics.

2.1. Definition of a mobile multibody system

A multibody system is a material system consisting of a set of material bodies connected to one another through internal joints, and to the rest of the world through external joints or contacts (modeled by punctual, surface, and/or volume densities of external forces and couples). Based on this basic model, we will first consider the case of multibody systems that consist of a finite set of rigid bodies, and then, in the next section (5), we will see how it is possible to extend this model to the rigid-but-continuous case and finally to soft robots with compliant organs. The conventional model of rigid multibody systems is well developed in the context of manipulation but much less so when dealing with locomotion. In contrast with classical multibody systems, any body included in a locomotion system will generally not only move relative to the other bodies but also perform rigid overall movements, i.e., make net displacements of its structure in the ambient space. Furthermore, these net motions are generally not imposed by explicit time laws, such as on a manipulator mounted on a wheeled platform or a mobile manipulator, but are produced at any given time by the contact forces applied to the whole system. We define this as the locomotion dynamics of the system. By extension of the current terminology, throughout this article we will term such a system a mobile multibody system, or MMS, to distinguish it from a classical multibody system, or MS. In spite of this semantic distinction, an MS is a particular case of MMS whose rigid overall motions are fixed through time laws, and the methodological framework that we will develop for the MMS would also be applicable to any MS. Finally, referring to the usual designs of robotics, 'mobile multibody systems' will include many robotic systems ranging from a fully constrained system (such as a wheeled platform) to a free-floating system (such as space shuttles and satellites) via conventional industrial manipulators, under-constrained nonholonomic systems (e.g., the snakeboard, the trikke), etc.

2.2. Configuration space of a mobile multibody system

Here we mean by 'Lagrangian' a theory that seeks to entirely derive the dynamics of a mechanical system from the knowledge of a unique function of its state, named the Lagrangian of the system. Mathematically, such a theory enjoys a solid geometric basis that has its roots in the theory of the Riemannian geometry of manifolds. In mechanics, the key definition of this model is the concept of a configuration manifold or, more simply, of a configuration space. The configuration space $\mathcal{C}$ of a material system is the geometric space whose points have for coordinates the kinematic parameters (also named 'generalized coordinates') of the material system. As a result, $\mathcal{C}$ is an abstract[3] space with a dimension equal to the number of degrees of freedom of the system. The generalized coordinates of the material system define for $\mathcal{C}$ a system of local coordinates, or 'charts', which gives $\mathcal{C}$ the structure of a manifold[4]. Any point of this abstract space corresponds to one (and only one) configuration[5] of the entire system in the ambient space $\mathbb{R}^3$. For a conventional MS, such as a manipulator with p revolute joints parameterized by the vector of joint angles[6] $r = (r_1, r_2, \ldots r_p)^T$, each r_i being the coordinate on a circle S^1, the configuration space is a hyper torus of dimension p defined by $\mathcal{C} = S^1 \times S^1 \times \ldots S^1 = (S^1)^p$. Thus any point of $\mathcal{C}$ corresponds to one configuration, or 'shape', of the MS in 3D space. In the case of MMSs, the parameterization of the system requires managing not only its shapes in relation to the previous space (which we name in this context 'shape space' and denote as $\mathcal{S}$) but also its absolute position and orientation in the ambient space. Hence, an MMS has internal degrees of freedom that define its shape and external degrees of freedom that correspond to its rigid overall position and orientation related to an external (inertial) frame fixed to space. In the Lagrangian picture of geometric mechanics, the external degrees of freedom are parameterized by the transformations g applying a frame fixed to ambient space on a frame moving with the MMS and defining the reference of net motions in space. This mobile frame is called the 'reference frame' and is generally attached to an arbitrarily distinguished body, named the reference body, of the entire MMS. Of course, the choice of this reference frame is not unique. For bio-inspired

[3] By 'abstract' we mean that this space is not the physical (ambient) space in which the material points of the system move.

[4] A (n-dimensional) manifold is a topological space (a set of points) locally identifiable to $\mathbb{R}^n$ thanks to a set of local charts covering it, and named an atlas (think of the earth, which is a two-dimensional manifold named S^2, with an atlas of local charts defined by geographic maps, which are pieces of $\mathbb{R}^2$) [78].

[5] In mechanics, a configuration is defined by the set of the positions of all the material points of the system in a frame attached to the ambient three-dimensional space (in brief, it is a snapshot of the system in the lab).

[6] Revolute joints are used for the purpose of illustration, but of course prismatic joints can also be considered.

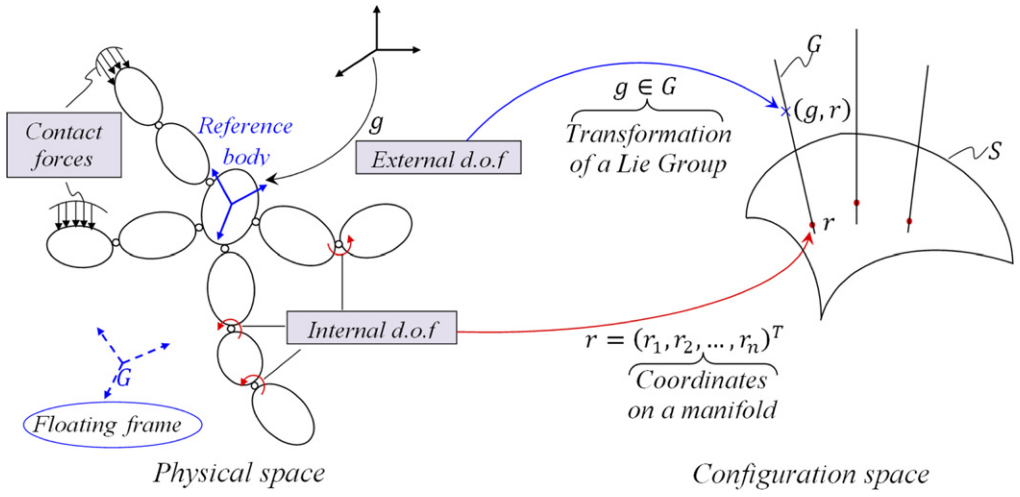

Figure 1. Configuration space of a locomotion system: the principal fiber bundle.

systems, it is often convenient to attach the reference frame to the body where exteroceptive sensors are located (unless 'embarked' is an industry-standard term). Alternatively, we can define such a frame as a basis of three independent vectors attached to one of the bodies (which is the reference body) but originating at a nonmaterial point such as the gravity center of the entire MMS. In this case, the reference frame floats in space, and we denote it as a 'floating frame' [21].

Geometrically, the transformations g, called 'net transformations', are the elements of a Lie group G, i.e., a group of transformations endowed with a manifold structure[7] [62]. There are several possibilities for defining such a group according to the case being considered. For example, when the reference frame undergoes one-dimensional translations, $G = \mathbb{R}$. For translations in a plane, $G = \mathbb{R}^2$. In the case of translations and rotations in a plane, G is called the group of Euclidean displacements in $\mathbb{R}^2$ and denoted G= SE(2). For translations in three-dimensional space, $G = \mathbb{R}^3$; and for rotations in three-dimensional space, G is the special orthogonal group G= SO(3). All these, and others, are included in the most general group G = SE(3), which defines the configuration space of a rigid body moving freely in 3D space. The transformation elements g of this group can be represented by the 4×4 homogeneous matrices:

$$g = \begin{pmatrix} R & p \\ 0 & 1 \end{pmatrix}, \tag{1}$$

where R and p respectively denote the rotational and the translational components of the transformation. In its group of configurations, a motion of a rigid body defines a time-parameterized curve $t \mapsto g(t)$ and any of its tangent vectors $\dot{g}$ defines a velocity of transformation. The composition hg of two transformations h and g acting in $\mathbb{R}^3$ corresponds in the group to a translation of g by h on the left, or of h by g on the right. For such translations that define nonlinear maps from points to points on G, we can compute their tangent linear maps (their Jacobian) and use them to translate the vectors tangent to the group (the velocities of transformation). For instance, taking the tangent map of the aforementioned left translation makes it possible to translate $\dot{g}$ from its base point g to any point hg of G and to obtain $h\dot{g}$. In particular, the left translation of $\dot{g}$ by $h = g^{-1}$ moves the base point of $\dot{g}$ from g to the unit (neutral) element 1 of G and defines the twist of the rigid body in its mobile frame, or 'material twist'[8] η, which we detail for G = SE(3) as:

$$g^{-1}\dot{g} = \begin{pmatrix} \Omega & V \\ 0 & 0 \end{pmatrix} = \eta, \tag{2}$$

where Ω and V denote the angular and linear velocities respectively of the body in its mobile frame[9]. The set of twists spans the tangent space to G at $g = 1$, denoted T_1G. After it is endowed with the commutator such that for any $\eta_1, \eta_2 \in T_1G$, $[\eta_1, \eta_2] = \eta_1\eta_2 - \eta_2\eta_1$, this space also defines the Lie algebra $\mathfrak{g}$ of the group G, denoted se(3) in the case of SE(3). Now that we have defined the geometric structures that make it possible to model the shape of an MMS (a point r in a manifold $\mathcal{S}$) and its net position and orientation (a point g on the Lie group of the reference body displacements G), we are able to introduce the definition of the configuration space of an MMS that endures both shape deformations and net rigid overall motions. Thus, in the case of an MMS as shown in figure 1, each

[7] The transformations g of G, which can be composed together with the internal composition law of G, are also points that can be localized in a chart of G. For instance, the Euler angles can be used to define the charts of the Lie group SO (3) of 3-D rotations.

[8] Material twists are sometimes called 'body-related twists' or, more simply, 'body-related velocities'.

[9] We do not distinguish a skew symmetric angular velocity matrix from its 3×1 vector. This is the same as in the case of SE(3), where the 4×4 matrix η is not distinguished from the 6×1 vector $(V^T, \Omega^T)^T$.

configuration of the system corresponds to a pair (g,r), which is a point of the configuration space:

$$C = G \times S. \tag{3}$$

Such a space (pictured in figure 1) is indeed well known in differential geometry as a 'principal fiber bundle'. In this theory, a bundle is a manifold defined (at least locally) as the direct product of a manifold called 'base manifold' and another space called 'fiber' that is endowed with an algebraic structure [78]. For example, if the fiber is a vector space, then the fiber bundle is a 'vector bundle' (more generally, a 'tensor bundle'). If, as is the case here, the fiber is a Lie group, then the fiber bundle is called a 'principal fiber bundle'. Finally, a rich corpus of results exists in geometric physics related to the structure of a fiber bundle where it plays a crucial role in, for instance, gauge theory and general relativity [35]. Hence, one of the strengths of the Lagrangian approach, some of whose key results we will review, is to have exploited this richness for the benefit of a locomotion theory in robotics. Particularly in the geometric model of physics, a geometrical object is intimately associated with the concept of the fiber bundle and even plays a more crucial role than that of the fiber bundle; this is the concept of 'connection'. However, before we introduce this concept and its use in locomotion, we will state the general problem that we will treat in this article.

3. General problem addressed in this article

The general problem of locomotion can be envisaged in several ways. In this article, we will address the following problem. Knowing the time evolution of the internal joints $t \mapsto r(t)$, we seek to compute:

1. The external net motions; this computation corresponds to solving the forward external dynamics, or 'forward locomotion model'
2. The internal joint torques; this computation corresponds to solving the inverse internal dynamics or, more simply, the 'inverse torque dynamics'

This computation is the purpose of the subsequent development. Before pursuing this line of reasoning, we will make a few remarks.

Remark 1.

– The first dynamics are termed the 'locomotion model' because, by relating the internal to the external d.o.f., they involve the model of contact forces, which are the fundamentals of locomotion. The second dynamics, or 'torque dynamics', are those usually encountered in a standard MS such as a manipulator, where they find their application in well-known computed torque algorithms.

– A natural question arises from this statement: why do we opt for the choice of internal motions as inputs? Why not take torques as input? There are two main reasons. First, it is an easy task to specify the motion of a locomotion robot in terms of its internal motion, but it is not at all easy to infer the joint torques that should be exerted by its actuators from the knowledge of the desired net motions. Second, this problem (and its solution) can be coupled with biological experiments based on locomotion films of animals. After internal motions have been extracted from such films, they can be imposed as inputs of the algorithm that feeds back the corresponding (modeled) external motions. These external motions can then be compared with the real ones extracted from the same films. The matching of measured and computed external motions is a valuable tool for the study of the contact model[10], which is by far the most difficult issue in locomotion dynamics modeling. In parallel, inverse torque dynamics allow us to assess the feasibility of imposed internal motions with respect to the resources of actuators.

– Another relevant problem related to locomotion is to invert the preceding locomotion model so as to find the internal shape motions that will produce given external net motions. The solution to this problem is related more to open loop control and can be used for motion planning or to seek locomotion gaits. This problem will not be dealt with further in this article. However, we note that the resulting inverse locomotion algorithm can be bypassed by addressing the open loop control as an optimization problem based on the use of the forward locomotion model that we present in this article. In this case, the idea consists of minimizing the error between actual and desired values of external motions with respect to the unknown shape motions [26].

Finally, the algorithmic solution to the general problem just stated is a useful tool for the design of gaits and transient maneuvers. Solving the forward external and internal dynamics (i.e., torques as input, internal and external motions as output) is of interest on its own in seeking to model passive internal deformations of constitutive bodies during compliant locomotion as will be addressed in section 9.

[10] This approach requires the position, velocities, and accelerations of both net and shape motions to first be measured and/or estimated. Second, knowing the inertia of the system, one can insert these kinematic variables in the dynamic balance equations of the net motions in order to infer the values of the external forces (all the other contributions to this balance being known inertial forces). For an illustration of this approach, see, for instance, [51] or [44].

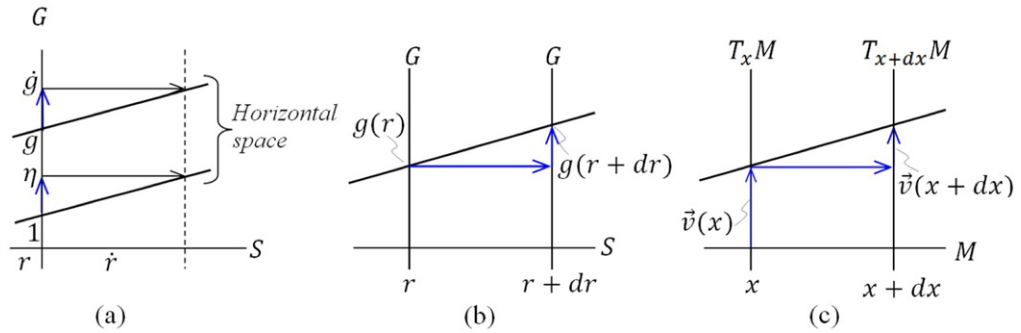

Figure 2. (a) Connection between motions ($\dot{r}$) in S and motions (η) in G; (b) principal fiber bundle $G \times S$; (c) tangent bundle TM of a manifold M.

4. Forward locomotion dynamics: the kinematic case

Based on these concepts, the shape motion of an MMS defines a motion of the manifold $\mathcal{S}$, whereas the net motion of its reference body defines a motion along Lie group G. Therefore, to solve the forward locomotion dynamics, we need to develop a relationship between these two types of motions of the principal fiber bundle $G \times \mathcal{S}$. In general, a dynamic model is required to develop such a relationship; i.e., the contact dynamics between the system and the surrounding medium must be solved, as we will discuss later in the next subsection. However, there is a particularly elegant case where locomotion is entirely defined by kinematics, i.e., through relationships between the shape and net velocities. This is when the model of the contact is encoded into what we call a connection with the principal fiber bundle of configurations [34]. In locomotion theory, such a connection exists when:

–(i) There is a linear relationship between a small (shape) displacement dr of $\mathcal{S}$ and a small (net) displacement dg of G.

–(ii) The corresponding material twist $g^{-1}dg$ is independent of g (left invariance).

Replacing 'small displacements' with velocities in this definition, a connection directly relates the net velocities[11] η to the (internal) shape velocities $\dot{r}$ through kinematics as follows:

$$\eta + \mathcal{A}(r)\dot{r} = 0. \tag{4}$$

For the principal fiber bundle, this context operates at any point (g,r) through $Ad_g(\eta + \mathcal{A}(r)\dot{r}) = 0$, which defines[12] the space of admissible velocities of the system or, in the language of differential geometry, a particular distribution of $\mathcal{C} = G \times \mathcal{S}$ called 'horizontal space', as illustrated in figure 2(a). In the literature on geometric mechanics, $\mathcal{A}(r)$ is known as the local connection 1-form or, more simply, the local form of the connection. It is a function of the shape variables r only by virtue of the condition (ii) previously mentioned. More generally, a connection univocally associates one element of a fiber over a point of the base manifold with another element of the fiber over a point that is infinitesimally close to the first one [29]. This pairing is illustrated in figure 2(b) for a principal fiber bundle and for the tangent bundle of a manifold M in figure 2(c). This latter context is well known in Riemannian geometry, where any metric is naturally associated with a connection ω known as a Levi-Civita connection, which transports in parallel any tangent vector on the manifold along the geodesics of the metric [24]. To illustrate such a Riemannian connection, we consider the case of the two-dimensional sphere S^2 endowed with the Euclidian metric induced from $\mathbb{R}^3$. Along any segment of a great circle (great circles are the geodesics of S^2), a vector tangent to the sphere can be transported in parallel from one point to another [7]. Finally, by considering any curve on S^2 as an infinite set of infinitesimally short pieces of geodesics, parallel transport can be defined along any curve on S^2, in particular when considering the case of closed curves starting and finishing at a same point on S^2. When any vector is transported in parallel along such a closed path, the vector after the entire transport appears to be shifted by a given angle θ with respect to its antecedent. By virtue of the Gauss–Bonnet theorem [78], this shift is in fact proportional to the area of the surface enclosed by the path and the curvature of the sphere (see figure 3(a)). In other words, this shift is a manifestation of the curvature of the manifold, and we have:

$$\theta = \int_{\text{Path}} \omega = \int_{\text{Enclosed area}} \mathrm{d}\omega, \tag{5}$$

which is just a particular case of the Stokes theorem, where $\mathrm{d}\omega$ is the curvature 2-form of the Riemannian

[11] They are defined in section 2.2 as the velocity of the reference body frame itself, i.e., in the case of SE(3) as (2) with g the configuration of the reference body.

[12] Ad_g is an operator called 'adjoint action of G'. It transports a twist from one frame to a second one, with g the transformation that maps the first on to the second frame.

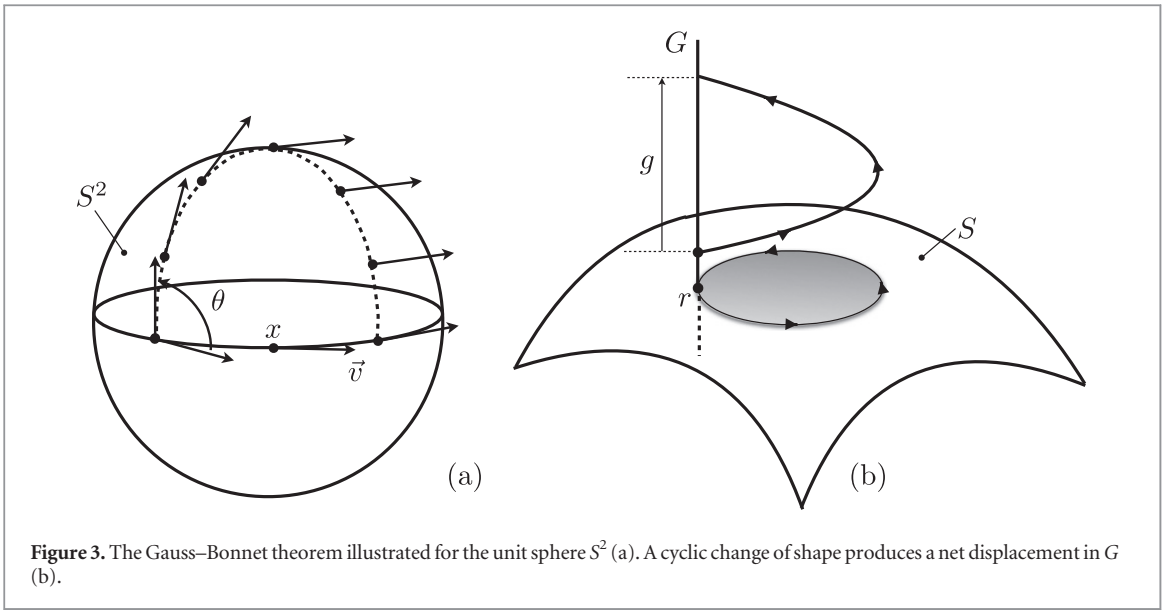

Figure 3. The Gauss–Bonnet theorem illustrated for the unit sphere S^2 (a). A cyclic change of shape produces a net displacement in G (b).

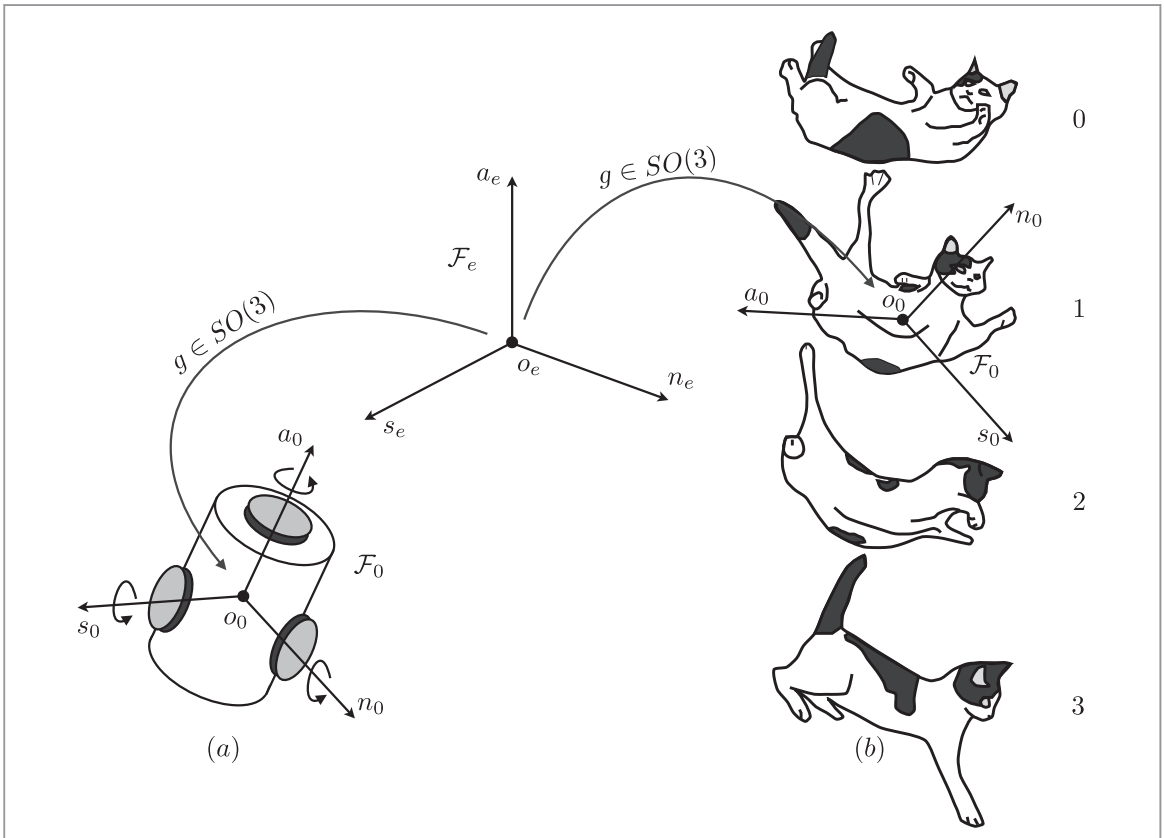

Figure 4. Mechanical connection: falling cat and orbiting satellite with rotors.

manifold. Remarkably, this geometric picture can be recovered in the case of the principal fiber bundle of an MMS when the fiber group is commutative (see figure 3(b)). In this case, we can associate with equation (4) a curvature 2-form named $d\mathcal{A}$ that relates the infinitesimally small closed paths in the shape space to the corresponding net displacements that they produce in the fiber [12]. This geometric picture is a valuable tool for gait generation in robotics [12, 42] because it gives a direct relationship between the cyclic shape motions of a given gait and the net displacement it produces. We will now review the two cases in robotics where forward locomotion dynamics can be modeled through kinematics using a connection.

Case 1: mechanical connection

We take the example of a free-falling cat or a satellite reorientation system as shown in figure 4. It is well known that a cat initially held with its four legs upward

and then dropped will reorient its head by twisting its body in a complex shape motion. At the end of its fall, the cat touches down in its initial shape but with its four legs on the ground. In doing so, the falling cat solves a problem of locomotion without any contact because the air has no influence at all on its motion. Like an orbiting satellite equipped with inertia wheels, the cat uses transfers of inertial momentum between its internal and external d.o.f. to reorient itself. From our geometric point of view, the configuration space of these systems (the cat and the satellite) is a principal fiber bundle $G \times \mathcal{S}$ with $\mathcal{S}$ the shape space of the cat skeleton or the three-dimensional torus in the case of the fully actuated satellite[13], and $G = \mathrm{SO}(3)$ in both systems. More precisely, we take the floating frame as the reference frame, which is centered on the gravity center of the system whose orientation with respect to a frame fixed to space is $R \in \mathrm{SO}(3)$. Then, according to the law of conservation of angular momentum, because no external forces are applied to the system, its total angular momentum remains null throughout the motion, i.e., $\sigma = 0$. In this case, the locomotion is therefore ruled by the following relationship:

$$\sigma = \sigma_{\mathrm{net}} + \sigma_{\mathrm{shape}} = 0, \tag{6}$$

where σ_{net} is the angular momentum due to the floating frame motions (i.e., the net reference motions of the MMS), and σ_{shape} is the angular momentum due to the internal shape motions. Further analysis gives the angular momentum as follows:

$$R^T\sigma = I_{\mathrm{lock}}(r)\Omega + I_r(r)\dot{r} = 0, \tag{7}$$

where Ω is the angular velocity of the reference frame in its mobile basis, I_{lock} is the angular inertia matrix of the system when it is rigidified in its current shape r, or 'locked inertia matrix' [12], and I_r is the inertia coupling matrix between internal and external accelerations. Given that the preceding relationship is left invariant (I_{lock} and I_r are R-independent) and linear with respect to the velocities, it defines a connection (2) with the following local form:

$$\mathcal{A}(r) = I_{\mathrm{lock}}^{-1}(r)I_r(r). \tag{8}$$

In the geometric mechanics literature, such a connection is known as a 'mechanical connection' [59]. It encodes all the information about the kinetic exchanges between the internal and external degrees of freedom. Referring to our introductive considerations about animal locomotion, the locomotion mechanism used by the cat is still a kind of action-reaction principle, but one in which the inertia (Coriolis and centrifugal) forces replace the external forces of the general context. In closing this example, we note that applying the same considerations to the translations of the floating frame and using the mass center theorem gives $\mathcal{A}(r) = 0$ because no external force is applied to the system. Thus, in this second case, the internal shape motions cannot act on the linear motions of the floating frame, which means that there is no 'connection' between these motions.

Case 2: kinematic connection

Now we consider the examples of an undulatory snake and a nonholonomic wheeled (unicycle) platform, as shown in figure 5. The reference frame is attached to the head of the snake and to the platform. Because both systems evolve in the plane, the principal fiber bundle of their configurations is $\mathrm{SE}(2) \times \mathcal{S}$, where $\mathcal{S}$ stands for the space of the snake skeleton in the one case and for the two-dimensional torus of the unicycle wheels in the other. Once again, a connection exists [48, 64, 74] between the internal shape motions and the external net motions of these two systems. This connection is generated by assuming that the contacts between the ground and the snakes's scales or the wheels are both modeled by ideal non-sliding (NS) and rolling without slipping (RWS) conditions[14]. To derive the expression of this connection, it suffices to insert the motion of the reference frame in the NS and RWS conditions and to bring together in both cases a set of three (=dim(SE(2))) independent nonholonomic constraints on the principal fiber bundle. In this way, we obtain the well = known kinematic model of wheeled mobile platforms of form (4), where once again the $\mathcal{A}(r)$ matrix, being independent of g, defines the local form of a connection known as the principal kinematic connection [12]. Note that in the case of a snake-like robot such as the Hirose ACM, this connection is built up from the lateral non-sliding constraints (the wheels being passive), whereas the unicycle platform must also use the rolling without slipping constraints of the two actuated wheels. These nonholonomic constraints are discussed in more detail in the next section, which deals in part with constrained systems.

5. Forward locomotion dynamics: the general case

As mentioned previously, in the general case, dynamics are required to solve the forward locomotion model. Due to the structure of the principal fiber bundle, the derivation of the dynamics requires special attention. In particular, the structure of the Lie group means that the standard variational calculus (on which the derivation of Lagrange's equations is based) applied to the charts of any manifold can be replaced by an intrinsic calculus applied directly to the group. Such a calculus has the advantage of formulating the dynamics with a minimum of nonlinearities. Indeed, in such an approach, all the nonlinearities induced by

[13] Note that in the case of a failure of inertia wheels, interesting problems of control accessibility arise.

[14] In the case of the snake, the strong frictional anisotropy of its skin along the axial and lateral directions justifies such assumptions.

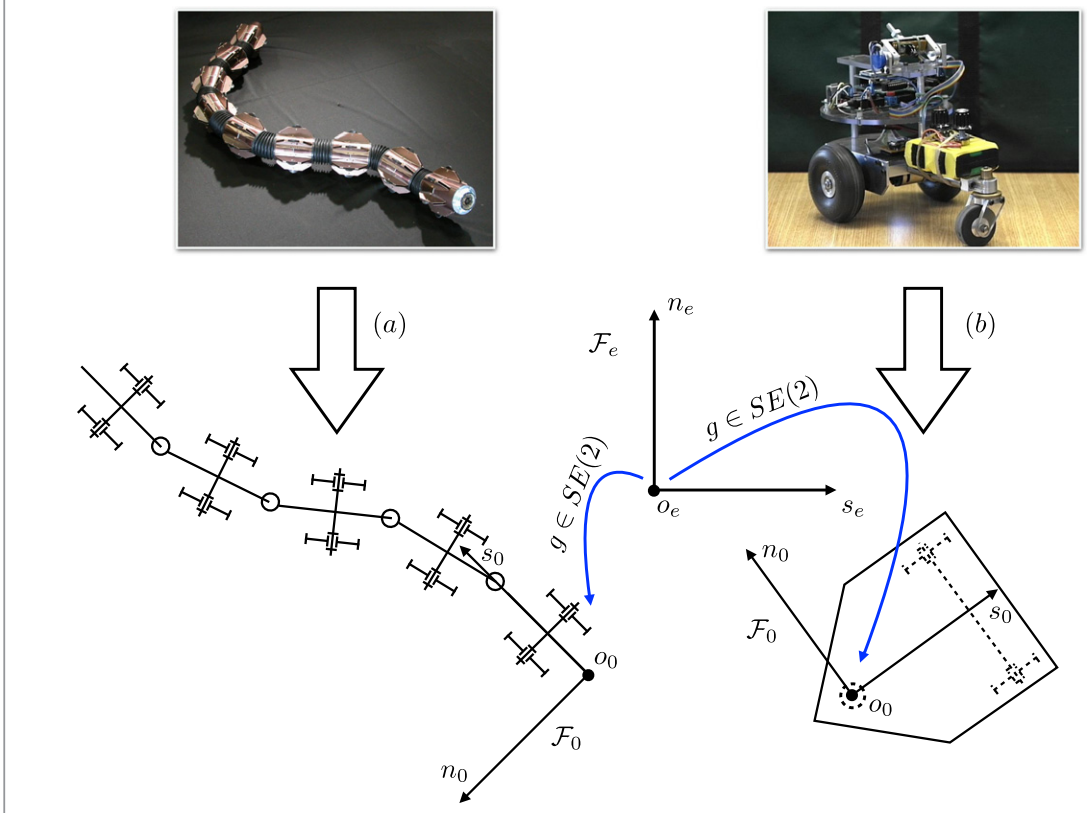

Figure 5. Kinematic systems: (a) the snake-like robot ACM-R5 from Hirose-Fukushima Robotics Lab (left) and (b) the nBot unicycle platform from the Geological Science Center of Southern Methodist University.

rigid motions are due to the curvature of the group (which can be intuitively considered as a geometric manifestation of the non-commutativity on the algebraic side) and not to any of its parameterizations. Euler explored this before the emergence of Lie groups starting from the case of the rigid top [6]. However, a long time passed before the geometric insight of the 'Eulerian' approach to dynamics was completely elucidated by Poincaré [65] followed by Chetayev [25], Rumyantsev [72], and Arnold [6] on the Russian side and by the American school of geometric mechanics after Marsden [56]. The idea of Poincaré[15] was to apply the Hamilton variational principle to the action of a system directly defined in terms of its transformations and not as a function of its parameters, which was the approach adopted by Lagrange [20]. According to this point of view, the action of the MMS is defined here as:

$$\int_{t_1}^{t_2} L\left(g, r, \dot{g}, \dot{r}\right) = \int_{t_1}^{t_2} \left(T\left(g, r, \dot{g}, \dot{r}\right) - U\left(g, r\right)\right) \mathrm{d}t, \quad (9)$$

where L, T, and U denote the Lagrangian, the kinetic energy, and the potential energy of the system, respectively, in the principal fiber bundle of its configurations. Then, using the Hamilton principle, the trajectory of the system between two fixed times t_1 and t_2 satisfies the stationarity condition in which $\forall\ \delta g$ s. t. $\delta g(t_1) = \delta g(t_2) = 0$:

$$\delta \int_{t_1}^{t_2} L\left(g, r, \dot{g}, \dot{r}\right) = -\int_{t_1}^{t_2} \delta W_{\text{ext}}\, \mathrm{d}t, \quad (10)$$

where δW_{ext} stands for the virtual work of the eventual external non-conservative forces exerted by the contacts. Now, replacing the virtual displacements and real velocities of transformation by the material twist of virtual displacements $\delta\zeta = g^{-1}\delta g$ and real velocities $\eta = g^{-1}\dot{g}$, and denoting $L(g, r, g\eta, \dot{r}) = l(g, r, \eta, \dot{r})$, we can restate the foregoing condition so that for any $\delta\zeta$ s. t. $\delta\zeta(t_1) = \delta\zeta(t_2) = 0$:

$$\delta \int_{t_1}^{t_2} l\left(g, r, \eta, \dot{r}\right)\mathrm{d}t = -\int_{t_1}^{t_2} \delta W_{\text{ext}}\, \mathrm{d}t, \quad (11)$$

where $\delta W_{\text{ext}} = \delta\zeta^T f_c$ and $l(g, r, \eta, \dot{r})$ is named the reduced left Lagrangian of the system, which takes the general form:

$$l\left(g, r, \eta, \dot{r}\right) = \frac{1}{2}\left(\eta^T, \dot{r}^T\right)\begin{pmatrix}\mathcal{M} & M\\ M^T & m\end{pmatrix}\begin{pmatrix}\eta\\ \dot{r}\end{pmatrix} - U\left(g, r\right), \quad (12)$$

where $\mathcal{M}$, M, and m are g-independent inertia matrices. Finally, when the potential energy U is independent of g, the Lagrangian is said to be left-invariant because in this case we have:

$$L\left(g, r, \dot{g}, \dot{r}\right) = L\left(hg, r, h\dot{g}, \dot{r}\right), \quad \forall\, h \in G, \quad (13)$$

[15] We assume here that the reader has basic knowledge of the derivation of Lagrange equations in generalized coordinates. Readers who are not interested in these aspects can skip to equation (16).

and in particular for $h = g^{-1}$, $L(1, r, g^{-1}\dot{g}, \dot{r}) = l(r, \eta, \dot{r})$. In the same way, any contact force f_c that does not explicitly depend on g is said to be left-invariant. This property is in fact a symmetry property frequently confirmed by the external forces exerted on an MMS. Now, to achieve the calculation of (11), we have to exploit two further properties, both resulting from the fact that the variation δ is applied while the time is kept fixed. First, r and $\dot{r}$ being considered as inputs known by their time evolution, we have $\delta r = \delta\dot{r} = 0$. Second, we necessarily have $\delta(\mathrm{d}g/\mathrm{d}t) = \mathrm{d}(\delta g)/\mathrm{d}t$, which leads to:

$$\delta\eta = \frac{\mathrm{d}\delta\zeta}{\mathrm{d}t} + [\eta, \delta\zeta]. \tag{14}$$

This relationship, which governs the commutation between variation and derivation, plays a key role in the variational calculus for Lie groups [65]. Indeed, it makes it possible to pursue the computation of (9) by the usual by-part integration as in the standard variational calculus attributed to Lagrange [36]. Finally, based on these properties, it is possible to show that any solution to the preceding variational principle is also a solution to the Poincaré equations [65]:

$$\frac{\mathrm{d}}{\mathrm{d}t}\left(\frac{\partial l}{\partial \eta}\right) - \mathrm{ad}^T_{\eta}\left(\frac{\partial l}{\partial \eta}\right) = X_g(U) + f_c, \tag{15}$$

where $\mathrm{ad}^T_{(.)}(.): \mathfrak{g} \times \mathfrak{g}^\star \to \mathfrak{g}^\star$ is the co-adjoint map of G, i.e., the dual map to the adjoint map[16] of $\mathfrak{g}$ on $\mathfrak{g}$ denoted $\mathrm{ad}_{(.)}(.)$ and defined by: $\mathrm{ad}_{\eta_1}(\eta_2) = [\eta_1, \eta_2]$; $X_g(U)$ models the conservative external forces, and $f_{\mathrm{ext}} = f_c + X_g(U)$. Note here that $X_g(U)$ accounts for the eventual symmetry defect of the Lagrangian system whose expression is detailed in [20] in its intrinsic form. Finally, applying (15) to the previously defined reduced Lagrangian gives the forward locomotion dynamics:

$$\begin{pmatrix}\dot{\eta}\\ \dot{g}\end{pmatrix} = \begin{pmatrix}\mathcal{M}^{-1}\mathcal{F}\\ g\eta\end{pmatrix}, \tag{16}$$

where $\mathcal{M}$ is called the locked inertia tensor because it corresponds to the inertia tensor of the MMS seen as a rigid body frozen in its current configuration, whereas in the same manner $\mathcal{F} = f_{\mathrm{ext}} + f_{\mathrm{inertial}}$ denotes the wrench of the locked external and inertial forces (including those induced by internal accelerations). The second line of the preceding state-space equation (16) forms the reconstruction equation that makes it possible to reconstruct, through a numerical time integration, the trajectory of the reference body $t \mapsto g(t)$ from the time evolution of η, which in turn is given by time integrating the first line of (16). Going further into the Lagrangian dynamics, the major difficulty now lies in the model of external forces, whose computation requires solving the dynamics of the physical contact between the system and the surroundings. This can be extremely difficult, as they are normally ruled by the properties of either:

- the ground (non-regular dynamics, tribology, etc).
- a fluid (involving Navier–Stokes equations).
- more exotic surroundings such as granular media (rheology).

For instance, in the case of swimming, the computation of f_{ext} requires the fluid dynamics to be solved at each time step of an integration loop. Obviously, such computations are incompatible with the real-time constraint imposed by robotics applications. Also, the art of physical modeling consists in solving this problem case by case. However, two subcases exist that require only geometry (and no physics) to solve the locomotion model. These geometric cases occur when f_{ext} is left-invariant and Lagrangian [11] or when f_{ext} is spanned by a set of Lagrange multipliers paired with constraints, i.e., when the contacts can be modeled by ideal kinematic constraints. We now briefly develop these two subcases and see how they are related to kinematic locomotion in a broader sense than that previously addressed in section 4.

Subcase 1: when the external forces are Lagrange multipliers of a set of kinematic constraints

We consider here the case where the contacts between the system and its surroundings (typically the ground) can be modeled through kinematic constraints. Practically, these constraints are deduced by forcing the velocity of the material points of the system in contact with the ground to be zero. According to Lagrangian mechanics, these constraints are imposed by Lagrange multipliers that are dual vectors of the velocities forced to zero [36]. As a result, in our case the Lagrange multipliers physically represent the external reaction forces transmitted to the system through the contact points[17]. This subclass of MMS plays an important role in locomotion on the ground by snake-like or walking robots. Indeed, in these cases the kinematic constraints imposed by the contacts can be expressed for the fiber bundle of configurations in the general form [13]:

$$0_m = A(r)\eta + B(r)\dot{r}, \tag{17}$$

where, if $n = dim(G)$, and m is the number of independent constraints imposed by the contacts, A and B are $m \times n$ and $m \times p$ matrices respectively, and 0_m is the $m \times 1$ zero vector. In this system of constraints, we encounter two cases that depend on the relative values of $rank(A)$ and n. In the first case, $rank(A) = n$ and (17) can be block-partitioned as:

[16] $\mathfrak{g}^\star$ denotes the dual space of the Lie algebra of material twists. It is the space of material wrenches f. In the case of G= SE(3), each f is a (6×1) vector gathering the resultant and the moment of forces exerted on a rigid body and expressed in its mobile frame, whereas ad_η is a (6×6) matrix whose detailed expression is given in [62].

[17] This also applies to angular velocities for which Lagrange multipliers are external reaction couples.

a b

Figure 6. Two under-constrained non holonomic systems: (left) the snakeboard; (right) the trikke.

$$\begin{pmatrix} 0_n \\ 0_{(m-n)} \end{pmatrix} = \begin{pmatrix} \overline{A} \\ \widetilde{A} \end{pmatrix} \eta + \begin{pmatrix} \overline{B} \\ \widetilde{B} \end{pmatrix} \dot{r}, \tag{18}$$

with $\overline{A}$ as an $n \times n$ square invertible matrix. In this case, given that the matrix $\overline{A}$ is invertible, η is completely defined by the time evolution $r(t)$ through the kinematic model $\eta = -\mathcal{A}\dot{r}$, where $\mathcal{A} = \overline{A}^{-1}\overline{B}$ defines the local form of a (kinematic) connection with the principal fiber bundle of configurations [66]. Furthermore, if $m = n$, then the mobile multibody system can move in any case; whereas if $m > n$, then the residual $m - n$ equations of (18) can be used to find the joint velocities $\dot{r}$, preserving the mobility of the entire system, i.e., verifying the following compatibility condition: $(\widetilde{B} - \widetilde{A}\mathcal{A})(r)\dot{r} = 0$, which admits the nontrivial solution ($\dot{r} \neq 0$) if mobility is possible. Finally, in this first case, there are enough independent constraints to permit replacing dynamics with kinematics. But in the second case, we have $rank\,(A) < n$, and the mechanism has insufficient constraints to define the net motions uniquely using kinematics, so further analysis is required. In this regard, applying generalized inversion to (17) allows one to state:

$$\eta = H(r)\eta_r + J(r)\dot{r}, \tag{19}$$

where, if $A^{(-1)}$ denotes a generalized inverse of matrix A, $J = -A^{(-1)}B$, and H is an $n \times (n - m)$ matrix whose columns span the kernel of A, i.e., of the locked constraints. As a consequence, η_r defines an $(n - m) \times 1$ vector called a reduced twist because it defines the twists that are compatible with the constraints. Now, by projecting the unconstrained dynamics (16) onto the kernel of the locked constraints, we obtain reduced dynamics:

$$\begin{pmatrix} \dot{\eta}_r \\ \dot{g} \end{pmatrix} = \begin{pmatrix} \mathcal{M}_r^{-1}\mathcal{F}_r \\ g\left(H\eta_r + J\dot{r}\right) \end{pmatrix}, \tag{20}$$

which rule the time evolution of η_r, and where $\mathcal{M}_r = H^T\mathcal{M}H$ and $\mathcal{F}_r = H^T(\mathcal{F} - \mathcal{M}(\dot{H}\eta_r + \dot{J}\dot{r} + J\ddot{r}))$.

Remark 2.

- When $J = 0$ and $H = 1$, we reproduce the unconstrained case (*case 1* of section 4), whereas when $H = 0$, the general kinematic model (19) degenerates into the kinematic case (*case 2* of section 4) with the kinematic connection $J = \mathcal{A}$. From this viewpoint, the kinematic case (*case 2* of section 4) and the dynamic one (*case 1* of section 4) are two extreme cases where the number of constraints induced by the contacts with the fiber bundle is respectively maximum and minimum. Indeed, in the first case the number of independent constraints is equal to the dimension of the fiber; whereas in the second, it is zero because the contacts introduce no constraint[18].
- Now it is easy to imagine MMSs that belong to the intermediate case where the system is constrained but with a set of constraints whose number does not exceed the dimension of the fiber. A particular case of such an MMS, relevant to robotics and also to sport biomechanics, is that which partially obeys kinetic exchanges between internal and external d. o.f. and partially those of kinematic contacts. Examples of MMSs ruled by such equations include all systems whose locomotion principle consists in transferring kinetic momentum from internal degrees of freedom to external ones via non holonomic constraints such as the snakeboard and the trikke (see figure 6), such as a skier sliding down a steep slope or an ice-skater performing a given choreography. In the latter case, the skater uses the mechanical connection when jumping into the air and a constrained version of it when in contact with the ice. These latter examples explain why, in Marsden *et al*'s original theory of Lagrangian

[18] This does not mean that the MMS does not contain any contacts. In fact, if there are some, they are modeled by forces that are themselves ruled by a physical contact law, e.g., of Coulomb.

locomotion, reduced twist η_r is replaced by a reduced momentum $p = \frac{\partial l}{\partial \eta_r}$, with l as the reduced Lagrangian (12), and the reconstruction equation is replaced by a connection equation [63].

– Wheeled snake-like robots such as the ACM robot are members of the class of over-constrained systems. In this case, their locomotion is entirely ruled by the kinematic connection $\mathcal{A} = \overline{A}^{-1}\overline{B}$. Moreover, constructing $\overline{A}$ with the first three constraints of the first three front links (each link having an axle) defines the net motions as a function of the first three joint motions. For the other joints, time integrating the residual compatibility equations allows one to obtain the follower-leader motion observed in the lateral undulation of snakes, where all the sections of the body track the path drawn by the snake head [63].

– A single system may exhibit several different cases while changing its configuration. For instance, in some singular configurations the rank of A can fall, resulting in a brutal shift from a case where the net motions are entirely defined by kinematics to another where dynamics are required. This case applies when the snake robot ACM has a constant curvature. Finally, walking robots present all the cases and subcases mentioned, including the unconstrained case (in the flying phase), the fully constrained case (in the single support phase), the over-constrained case (in the double support phase), and even the under-constrained case (in more exotic cases such as dancing on points or when using degenerate models of a foot) [38].

– It is worth noting that the computation of the net motions from the internal ones does not mean that these motions are feasible. The actuators must be able to supply the internal desired torques to ensure the feasibility of these motions. In the same vein, in the case of unilateral constraints, as in the case of legged locomotion or snake lateral undulation in trees, the bilateral constraints of (17) have to be activated or deactivated depending on the sign of the reaction forces they transmit. These points will be evoked in the next section, which deals with torque computation.

– A contact is impact-less when the kinematic constraint it introduces is satisfied just before the contact occurs. (This is the case of a snake smoothly changing its supports in lateral undulation.) In this case, the former context, which comes into the realm of smooth dynamics, is valid. However, when the constraint is not satisfied before the contact occurs, as in the case of legged locomotion, it generates an impact that can be modeled by changing the dynamic balance of forces of the system (16) into abalance of kinetic momentums using the concept of impulse and restitution coefficients, or alternatively by using a smooth model of the contact forces as a function of deformations between the legs and the ground [27].

– In [15], the preceding context has been extended to the case of systems having passive internal degrees of freedom such as those introduced by passive wheels and compliant organs whose deformations are described in the floating frame approach of flexible multibody system dynamics [21]. In this case, the passive internal velocities are brought together with the external ones in (19) and (20), whereas the kernel of admissible velocities now contains internal motions whose evolution requires a dynamic model.

Subcase 2: when the external forces derive from a (left-invariant) Lagrangian

This case was first introduced by Birkhoff in [11]. It means that a Lagrangian function $l_{\text{ext}}(r, \eta, \dot{r})$ exists such that:

$$F_{\text{ext}} = -\frac{\mathrm{d}}{\mathrm{d}t}\left(\frac{\partial l_{\text{ext}}}{\partial \eta}\right) + \mathrm{ad}^T_\eta\left(\frac{\partial l_{\text{ext}}}{\partial \eta}\right), \tag{21}$$

so that the dynamic locomotion model can then be rewritten as follows:

$$\frac{\mathrm{d}}{\mathrm{d}t}\left(\frac{\partial\left(l + l_{\text{ext}}\right)}{\partial \eta}\right) - \mathrm{ad}^T_\eta\left(\frac{\partial\left(l + l_{\text{ext}}\right)}{\partial \eta}\right) = 0.$$

Furthermore, if the system starts at rest, i.e., if we have the following situation at $t = 0$: $\partial(l + l_{\text{ext}})/\partial\eta = 0$, then:

$$\frac{\partial\left(l + l_{\text{ext}}\right)}{\partial \eta} = 0, \quad \forall\, t > 0. \tag{22}$$

For example, in the case of 3D swimming at a high Reynolds number, if an MMS is immersed in an ideal fluid with no vorticity and initially at rest, the hydrodynamic forces exerted onto the system derive from a Lagrangian function that is equal to the added kinetic energy[19] of the corresponding potential flow [52]:

$$l_{\text{ext}}\left(g, r, \eta, \dot{r}\right) = \frac{1}{2}\left(\eta^T, \dot{r}^T\right)\begin{pmatrix}\mathcal{M}_{\text{add}} & M_{\text{add}}\\ M^T_{\text{add}} & m_{\text{add}}\end{pmatrix}\begin{pmatrix}\eta\\ \dot{r}\end{pmatrix},$$

which implies, using (22) with l having the form of (12) and $U = 0$, the conservation law of kinetic wrench:

$$\tilde{\mathcal{M}}\eta + \tilde{M}\dot{r} = 0, \tag{23}$$

where $\tilde{\mathcal{M}} = \mathcal{M} + \mathcal{M}_{\text{add}}$ and $\tilde{M} = M + M_{\text{add}}$. We then recover the same structure as that of the falling cat, i.e., a kinematic model of form (4), with $\mathcal{A} = \tilde{\mathcal{M}}^{-1}\tilde{M}$. This connection is sometimes called the

[19] The term 'added' means here that this kinetic energy corresponds to the fluid mass accelerated with the body, in such a manner that it can be simply added to the body mass.

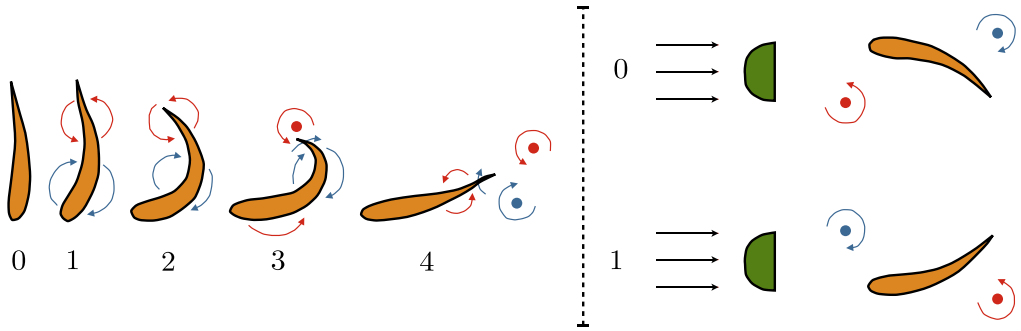

Figure 7. Swimming fish: (left) a fish turns by controlling vorticity. (right) A fish swims downstream from a bluff (lunate-shaped) body. The vortices are drawn as dots surrounded by oriented circles.

'hydrodynamic connection' because it encodes the kinetic momentum exchanges between the body and the surrounding fluid [47, 49, 55, 58].

Remark 3.

- Because in (23) $\eta \in \mathfrak{se}(3)$ and the mass matrices are not sparse, the hydrodynamic connection, in contrast with the mechanical connection of the free-falling cat or the orbiting satellite, can change both the position and the orientation of the system. As a result, this simple model can explain how, at high Reynolds, an MMS can swim in a quiescent fluid.
- Swimming at low Reynolds can also be modeled using the Stokes connection [40]. In fact, this context was the first application of gauge theory, relative to the principal fiber bundle, to a case of animal locomotion by Shapere and Wilczek [75]. Intuition suggests that in this case the inertial forces exerted on the body by the fluid are negligible compared with the viscous ones. Thus the resultant of viscous forces, which are essentially proportional to the body velocity field, is zero. When expressed in the principal bundle of configurations, these velocities are linear with respect to $\dot{r}$ and η, thus leading to the Stokes connection.
- The well-known 'scallop theorem' states that any animal with only one internal degree of freedom cannot move in a quiescent ideal fluid [69]. In fact, by opening its shell, such a 'mathematical scallop' would lose the net displacement it would gain by closing it, resulting in zero net motion after one cycle. Modeling this locomotion mode using the 'hydrodynamic connection' allows a straightforward geometric interpretation of this result. In fact, invoking the Gauss–Bonnet picture of section 4, a closed path on a one-dimensional $\mathcal{S}$ encloses a surface of null area, resulting in a zero net displacement after one cycle.
- In a real viscous fluid, the sharpness of the scallop's shell edge produces vorticity, which generates kinetic momentum variations. Indeed, the 'body + fluid' kinetic momentum conservation law can be extended to the case of rotational flows by adding a vorticity contribution to the balance of wrenches (23) [46]. In this case, the balance of kinetic momentum applied to the 'body + fluid' system takes the form of the sum of wrenches (linear and angular momentum noted as w):

$$\begin{pmatrix} p_{\text{shape}} \\ \sigma_{\text{shape}} \end{pmatrix} + \begin{pmatrix} p_{\text{net}} \\ \sigma_{\text{net}} \end{pmatrix} + \begin{pmatrix} p_v \\ \sigma_v \end{pmatrix} = \begin{pmatrix} 0 \\ 0 \end{pmatrix}, \qquad (24)$$

where the two first terms are those involved in the potential flow context but expressed in the fixed frame, i.e., $Ad_g^{-T}(\tilde{\mathcal{M}}\eta + \tilde{M}\dot{r}) = w_{sh} + w_{\text{net}}$, whereas the third term defines the contribution of the vorticity to the kinematic momentum balance:

$$\begin{pmatrix} p_v \\ \sigma_v \end{pmatrix} = \begin{pmatrix} \int_{\partial B} x \times \left(n \times u_\omega\right) \mathrm{d}a + \frac{1}{2}\int_F x \times \omega \mathrm{d}v \\ -\frac{1}{2}\int_{\partial B} x^2 \left(n \times u_\omega\right) - \frac{1}{2}\int_F x^2 \omega \mathrm{d}v \end{pmatrix},$$

with $\times$ the cross product in $\mathbb{R}^3$, ω the vorticity field, u_ω the fluid velocity induced (through a Helmoltz-like relationship) by the vorticity field, and x the position vector in the fixed frame. In nature, most flying or swimming animals not only generate vorticity around them but control it to produce thrust, lift, or steering moment. Mathematically, they use the first term of (24) to generate and control[20] the third term of (24) and finally to control the second (net motions). As an illustration, we consider the fish in figure 7. When turning, the fish first bends its body (thus modifying w_{shape}). This creates a rotational structure, called a protovortex, around it [60, 61]. While moving forward, the protovortex sweeps past the body before it reaches the trailing edge of the caudal fin, where it becomes an actual vortex that is shed in the wake (modeled by w_v).

[20] It is worth noting here that whereas (24) can model the transfers of kinetic momentum between the body and the vorticity in its surroundings, it cannot explain vorticity generation itself, which requires a model of the boundary layers where vorticity is produced.

After the vortex is shed in the wake, the appearance of an additional vortical term in the conservation law modifies the component w_{net} and makes the fish turn. More generally, animals generate vorticity to generate lift used for sustentation and thrust against drag and gravity. For proof of the relationship between vorticity and lift, we recall the basic Kutta picture of aerodynamics where a starting vortex shed behind a rigid wing generates a circulation around it and finally a lift proportional to this circulation. More recently, biologists and hydrodynamicists have discovered that animals can interact with the surrounding vorticity to preserve usable energy for locomotion. This is the case of a fish interacting with its own wake in order to extract an energy that would be wasted otherwise [80] or of a moth recapturing a vortex shed at each passage of the wing [33]. More remarkably, a dead fish placed in a Karman vortex street can swim upstream without producing any energy, i.e., in a purely passive way [9]. This famous experiment is pictured in figure 7 and will be illustratedfurther when we deal with the numerical implementation of these models.

6. Inverse torque dynamics

Here we discuss the second model, i.e., the torque dynamics of section 3, which compute the internal torques of the locomotion system. Because $(g, \eta, \dot{\eta})$ can be computed at each instant from the resolution of the locomotion dynamics (see the preceding section), we are potentially able to reconstruct the internal torques required at each instant of the movement. For that purpose, we reconsider the Lagrangian (12) to which we apply the Poincaré equations with respect to the Lie group $G \times \mathbb{R}^n$, where $\mathbb{R}^n$ is a coordinate system over $\mathcal{S}$. This gives the following dynamics:

$$\begin{pmatrix} \mathcal{M} & M^T \\ M & m \end{pmatrix} \begin{pmatrix} \dot{\eta} \\ \ddot{r} \end{pmatrix} = \begin{pmatrix} f \\ Q + \tau \end{pmatrix} + \begin{pmatrix} f_{\text{ext}} \\ Q_{\text{ext}} \end{pmatrix}, \qquad (25)$$

where we recognize in the first (top) row the external dynamics with r now governed by the second (down) row of (25) (i.e., the internal (shape) dynamics), from which we can extract the expression of the control torques:

$$\tau = M\left(\mathcal{M}^{-1}\mathcal{F}\right) + m\ddot{r} - Q - Q_{\text{ext}}, \qquad (26)$$

where we have used the expression of the net accelerations given by (16). In particular, in the constrained case where the external forces are produced by Lagrange multipliers, we have $f_{\text{ext}} = A^T\lambda$ and $Q_{\text{ext}} = B^T\lambda$, with λ the set of reaction forces forcing the constraints (17). As a result, a generalized inversion of the first row of (25) gives:

$$\lambda = (A^T)^{(-1)}\, h\left(r, \dot{r}, \ddot{r}\right) + \lambda_{\text{stat}} = \lambda_{\text{kin}} + \lambda_{\text{stat}}, \qquad (27)$$

with $h = \mathcal{M}\dot{\eta} - f + M^T\ddot{r}$ and $\dot{\eta}$ given by the time differentiation of (19). Re-injecting (27) in the second row of (25) gives:

$$\tau = M\dot{\eta} + m\ddot{r} - Q - B^T\left(\lambda_{\text{kin}} + \lambda_{\text{stat}}\right) = \tau_{\text{kin}} + \tau_{\text{stat}}, \qquad (28)$$

where τ_{kin} is the kinematic component of the total torque entirely explainable by the motion, whereas $\tau_{\text{stat}} = -B^T\lambda_{\text{stat}}$ (with $\lambda_{\text{stat}} \in \text{Ker}(A^T)$) corresponds to static loadings, which do not produce any observable net motion. In fact, they generate the internal stresses experienced by the robot due to the hyperstatism of the contacts. These internal stresses are available as an additional degree of freedom of locomotion and can be modulated to enhance such criteria as adherence. Referring to the last remark of section 5 (*subcase 2*), these internal stresses can be chosen to make the motion dynamically feasible. For instance, when the contacts are unilateral, as in the case of the snake's lateral undulation, the snake can play with its λ_{stat} in order to preserve the sign of each component of λ; otherwise, it has to change its supports and remove the corresponding constraint from (17). In [15], the inverse internal dynamics (28) have been extended to the case of systems containing internal passive degrees of freedom.

7. Practical implementation

Up to now, the general dynamic problem stated in section 3 has been addressed with Lagrangian models. Although such models are suited to analysis and classification, when addressing the problem of fast simulation and control of locomotion dynamics, the Newton–Euler model is preferred. Such a model has the same physical content as the Lagrangian one. However, it is derived from another definition of the configuration space of the MMS, which is no longer that of principal fiber bundle (3) but rather $C = G \times G \times \ldots G$, where each copy of $G\,(= \text{SE}(3))$ stands for the configuration group of each of the constitutive bodies of the systems, considered individually. To derive this model, we can apply the Poincaré equations to the reduced Lagrangian of each of the bodies; or, more simply, one can apply Newton's law and the Euler theorem of kinetic momentum. Because the bodies are isolated, they are mathematically reassembled by a kinematic model of the joints, and the model takes the form of the following set of differential algebraic equations, with $j = 0, 1 \ldots n_b$ and $n_b + 1$ being the number of bodies in the system:

$$\mathcal{M}_j\dot{\eta}_j = \text{ad}^T_{\eta_j}\left(\mathcal{M}_j\eta_j\right) + f_{ext,j} + f_j - \sum_{i/j=a\,(i)} Ad^T_{g_{i,j}} f_i, \qquad (29)$$

$$g_j = g_i g_{i,j}, \qquad (30)$$

$$\eta_j = Ad_{g_{i,j}}\eta_i + A_j\dot{r}_j, \qquad (31)$$

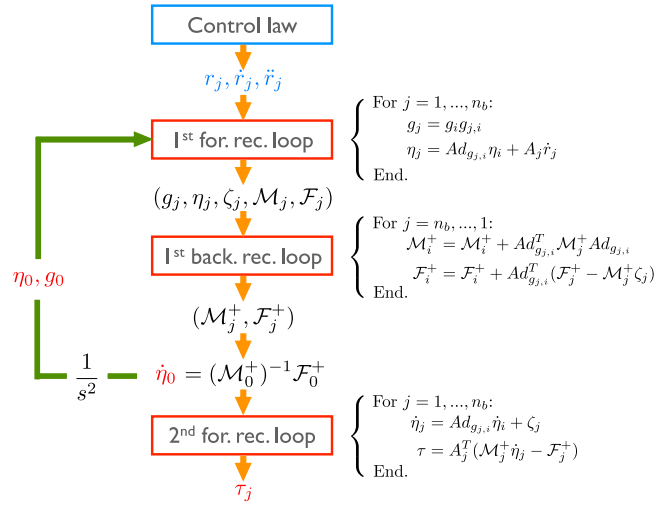

Figure 8. Flowchart of the Newton–Euler-based inverse dynamics algorithm for a tree-like MMS (the inputs are in blue; the outputs are in red). $\mathcal{M}_j^+$ and $\mathcal{F}_j^+$ denote the inertia matrices and the forces applied to a rigid body composed of all the bodies after the jth one, when the joints are locked in their current configuration [67].

Table 1. Asymptotic correspondence between discrete and continuous MMSs.

	Continuous
Discrete mobile MS	MMS = Cosserat beam
Rigid body	Cross-sections
Vertebral column (backbone)	Beam centroidal line
Discrete body indices j	Beam sections labeled X
Joint coordinates r_j	Strain field ξ
Interbody forces f_j	Stress field f

$$\dot{\eta}_j = Ad_{g_{i,j}}\dot{\eta}_i + \zeta_j\left(\dot{r}_j, \ddot{r}_j\right), \tag{32}$$

where $a(j)$ is the number of the bodies located just before the body $\mathcal{B}_j$ when descending the chain from the reference body to the tip branches ('a' means 'antecedent'). Due to the tree-like topology, labeling the bodies in an increasing order from the reference body $\mathcal{B}_0$ to the tips of the branches gives this set of equations a recursive nature with respect to the bodies index[21]. To be convinced of this, we point out that with this labeling, and knowing the time evolution of the joint and external positions, velocities and accelerations $t \mapsto (g, \eta, \dot{\eta})(t)$ and $t \mapsto (r, \dot{r}, \ddot{r})(t)$, (30)–(32) can be used as forward recursions to compute $(g_j, \eta_j, \dot{\eta}_j)$, $j = 1, .. n_b$ at each step of a time loop, whereas (29) can be used as a backward recursion on inter-body forces to compute $(f_{n_b}, f_{n_b-1} ... f_1)$ and finally the external force f_0 applied to $\mathcal{B}_0$; whereas projecting $f_1, f_2 .. f_{n_b}$ on to the joint axis gives the joint torques. As a result, this simple algorithm solves the inverse external and internal dynamics. When addressing the inverse internal and forward external dynamics problem of section 3, the time evolution of the net acceleration $\dot{\eta}$ is not known but must be computed by the algorithm. In figure 8, the flowchart of the recursive algorithm that solves this problem for any unconstrained rigid tree-like MMS is given as it has been introduced in [50] for open chain systems. In this second algorithm, the joint torques are computed with a forward recursion, whereas an additional recursion (called the first backward recursion) recursively computes the matrices $\mathcal{M}$ and $\mathcal{F}$ (here noted as $\mathcal{M}_0^+$ and $\mathcal{F}_0^+$) of the external dynamics (16) from which the current net acceleration $\dot{\eta}$ (noted $\dot{\eta}_0$ in the algorithm) is computed. This algorithm has been adapted for the case of constrained systems such as non holonomic snakes in [13] and more recently for constrained systems with passive internal d.o.f. [15]. When used for computations, the NE formulation enjoys many advantages compared with Lagrange models. First, equations (29)–(32) can be written by hand on a single page, whereas their Lagrangian counterparts, (16) and (26), require heavy symbolic computations. Second, they can be easily implemented on a computer through simple loops on the body indices. The resulting algorithms are fast and have an $o(n_b)$ complexity (n_b being the total number of joints), a desirable feature in the case of complex bio-inspired systems. Last but not least, NE models can be naturally generalized to the case of continuous MMSs, as will be discussed in the next section.

8. From discrete to continuous systems

For the sake of simplicity and until further notice, we will restrict our attention to the case of mono-branch (open chain) systems. Making the number of bodies increase while their length (along the unique branch) decreases in the model of discrete MMSs of section 2 asymptotically defines a model for continuous MMSs. The correspondence between discrete and continuous

[21] Note that with this labeling, $(g_0, \eta_0, \dot{\eta}_0) = (g, \eta, \dot{\eta})$.

systems is given in table 1. As was previously the case for discrete MMSs, the internal d.o.f. parameterized by the strain field ξ along the X-vertebral axis are governed by time-dependent functions $t \mapsto \xi(t)$ modeling the local shape deformations imposed by the control along with the internal constraints imposed by the design. The resulting model is that of rigid continuous elongated systems. It is well suited for modeling hyper-redundant vertebrates, such as snakes, or animals, such as fish, having a continuously controlled shape along their vertebral axis. Furthermore, with slight adaptations, this model can be used to model soft elongated hydrostats such as worms or caterpillars [14]. Applying the asymptotic process outlined in table 1 makes it possible to state the NE model of an open chain continuous MMS under the following set of partial differential equations (PDEs):

$$\mathcal{M}\dot{\eta} = \mathrm{ad}_{\eta}^{T}(\mathcal{M}\eta) + f_{\mathrm{ext}} + f' - \mathrm{ad}_{\xi}^{T}(f), \tag{33}$$

$$g' = g\xi, \tag{34}$$

$$\eta' = -\mathrm{ad}_{\xi}(\eta) + \dot{\xi}, \tag{35}$$

$$\dot{\eta}' = -\mathrm{ad}_{\dot{\xi}}(\eta) - \mathrm{ad}_{\xi}\left(\dot{\eta}\right) + \ddot{\xi}. \tag{36}$$

Equations (33)–(36) can be derived from an extension of Poincaré equations to continuous systems called Poincaré–Cosserat equations [19] or by applying the Newton–Euler theorems to each of the isolated cross-sections. In any case, they stand for the dynamics of the beam in a configuration space defined as a set of X-parameterized curves in group G of a rigid cross-section. For instance, in the case of a three-dimensional beam of unit length, $\mathcal{C}$ is the functional space $\{g(.): X \in [0, 1] \mapsto g(X) \in \mathrm{SE}(3)\}$. The three other sets of equations (34)–(36) are constraints that represent the model of the transformations and their velocities and accelerations along the body as a function of the imposed strain field ξ and its time derivatives $(\dot{\xi}, \ddot{\xi})$. As a result, we can add to the correspondence table 1 a left column with equations (29)–(32) and a right column with (33)–(36).

Finally, the generalization of the algorithm in figure 8 from discrete systems to the case of (open chain) continuous systems has received a solution in [18] and has been used to study fish swimming [19, 22] as well as the terrestrial locomotion of elongated animals such as snakes and worms [14], along with hovering flight [10]. For the purpose of illustration, some of these results are displayed in figure 10. This algorithm, whose flowchart is displayed in figure 9, is the transposition of the discrete algorithm in figure 8 where the recurrences in discrete body indices are replaced by ordinary differential equations for X and where the set of interbody forces (which contain the output torques τ) is replaced by a field of internal stress f, forcing (as a set of Lagrange multipliers does) the imposed time evolutions $t \mapsto (\xi(t), \dot{\xi}(t), \ddot{\xi}(t))$ along the X-axis. Finally, by combining the discrete and continuous models (29)–(32) and (33)–(36), we can find an NE model of a tree-like structure with continuous branches, a model that can be applied to hydrostats of more complex topology such as octopuses. Furthermore, such a model is the basis of a dynamic model of systems containing soft appendages, as we will see in the next section.

9. Toward soft systems

We now turn to the case of systems containing compliant bodies. If deformation is applied along a dominant axis of such a body, we can apply to this body the previous model of a continuous robot . However, in this case, ξ is no longer a prescribed function of time forced by the field of Lagrange multipliers f as in the dynamic problem of the preceding section but rather is governed by strain–stress relationships of the form:

$$f = \mathcal{R}\left(X, \xi, \dot{\xi}\right). \tag{37}$$

With these additional rheological laws, the model (33)–(36) becomes that of a geometrically exact[22] (Cosserat) beam [76]. In particular, considering a hyper-elastic material governed by Hook's law, the following simple form is imposed on (37)[23]:

$$f = H\left(\xi - \xi_o\right), \tag{38}$$

which changes the strain-controlled PDEs (33) (where $\xi = \xi(t)$) into a famous set of nonlinear beam equations due to Reissner [70], which, for a circular cross-sectional beam, can be detailed as:

$$\begin{cases} \rho A\left(\dfrac{\partial V}{\partial t} + \Omega \times V\right) = \dfrac{\partial N}{\partial X} + K \times N + N_{\mathrm{ext}}, \\ \rho J\dfrac{\partial \Omega}{\partial t} + \Omega \times \rho J\Omega = \dfrac{\partial M}{\partial X} + K \times M + \Gamma \times N + M_{\mathrm{ext}}. \end{cases} \tag{39}$$

Starting from this general model[24], part of the components of f can be Lagrange multipliers forcing rigid internal constraints, such as those changing a Reissner beam into a Kirchhoff beam or into an unstretchable Kirchhoff beam[25]. Now, because the stress field ruled by (37) is function of the current state,

[22] The term 'geometrically exact' means that the deformations of the beam centroid line and the rotations of its cross-sections are modeled in an exact manner, contrary to the linearized beam theories used in strength of material for engineers.

[23] H is a 6×6 tensor modeling the Hook's law beam and $\xi_o = (1, 0, 0, 0, 0, 0)^T$ is the value of ξ when the beam is in its configuration at rest, which is assumed to be straight.

[24] Where the general terms of (33) take the particular form $\mathcal{M} = \mathrm{diag}(\rho A 1_{3\times 3}, \rho J) = \mathrm{diag}(\rho A, \rho A, \rho A, \rho I_\rho, \rho I, \rho I)$, $f_{\mathrm{ext}} = (N_{\mathrm{ext}}^T, M_{\mathrm{ext}}^T)^T$, $\xi = (\Gamma^T, K^T)^T$, $\Gamma = R^T(\partial p/\partial X)$, $K = R^T(\partial R/\partial X)$ ($R(X)$ and $p(X)$ being defined by (1) for each X-beam cross-section), and $H = \mathrm{diag}(EA, GA, GA, GI_\rho, EI, EI)$, with E and G the Young and twisting modulus of the beam material, ρ its density, and A I, and I_ρ the area and the axial and polar momentum of the beam cross-section.

[25] The corresponding components of f are defined in the same way as in the dynamic problem of the preceding section.

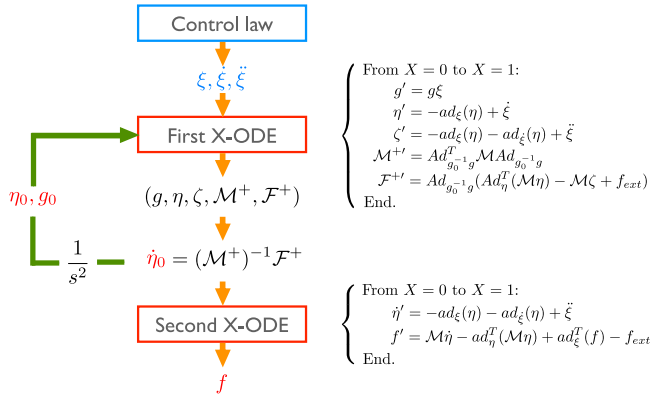

Figure 9. Flowchart of the continuous dynamics algorithm solving the dynamic problem stated in section 3 for a hyper-redundant robot. In contrast with the discrete case, the first two recursive computations in figure 8 are brought together in a unique ordinary differential equation (ODE) X-integrated from $X = 0$ to 1.

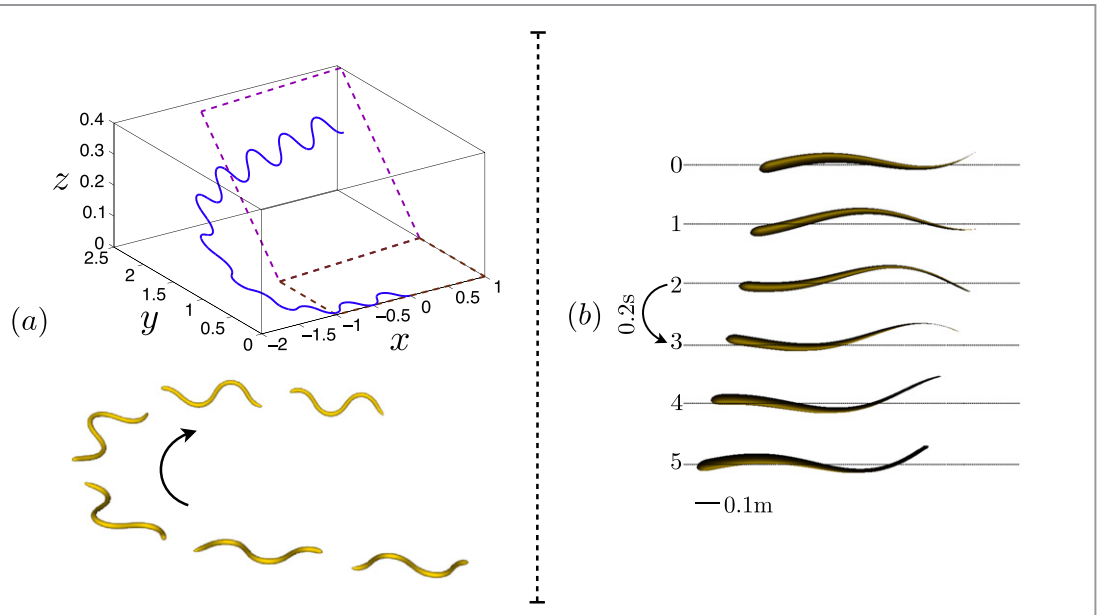

Figure 10. (left) Turning maneuver of a continuous snake in 3D lateral undulation: head trajectory (top left) and snapshots (bottom left). (right) Body-caudal fin swimming of a self-propelled fish according to Lighthill's large-amplitude elongated-body theory [22]. The snake and the fish are modeled by an internally actuated Cosserat beam [14, 22] and simulated using the algorithm of figure 9.

when it is computed in a time-integration loop, it introduces known variables, taking the meaning of torque inputs in a forward dynamics algorithm. Ideally, we would like to solve these forward continuous dynamics with a forward version of the algorithm of continuous systems in figure 9. Unfortunately, such an algorithm has not been obtained to date. In [17], we proposed an alternative solution based on the preliminary discretization of the beam into rigid bodies to which the discrete forward dynamics algorithm is applied. This algorithm, whose flowchart is given in figure 11, has been illustrated in the case of hovering flight [67], the passive swimming of a dead fish [23], and, more recently, a real fish-like robot [68]. Some of these results are displayed in figure 12. Finally, we note that from the point of view of continuous media mechanics, in the Cosserat approach, the body deformations are measured with respect to certain Galilean fixed reference configurations. As a result, to cope with the finite rigid overall transformations, the strain measurements are nonlinear (left-invariant), and in this case, most of the geometric nonlinearities appear through strain energy according to what we have called, since the works of Simo [77], the 'geometrically exact approach' to nonlinear structural dynamics. Alternatively, one can adopt mobile reference configurations instead of fixed ones. This is the choice adopted by the so-called floating frame approach, in which the body deformations are measured with respect to certain rigid floating (and fictitious) bodies, which follow the real deformed ones [21]. In this approach, the strain measurements are generally linear and the deformation fields that map the floating bodies onto the deformed ones can be

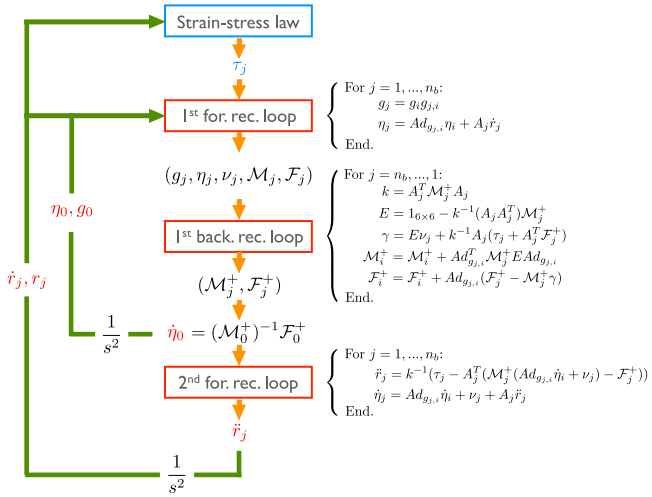

Figure 11. Flowchart of the Newton–Euler-based forward dynamics algorithm for a tree-like MMS. We note that $\zeta_j(\dot{r}_j, 0) = \nu_j$, whereas the strain–stress relations of (37) are discretized into spring-damper torques that are fed back to the joints at each time step of the simulation loop [67].

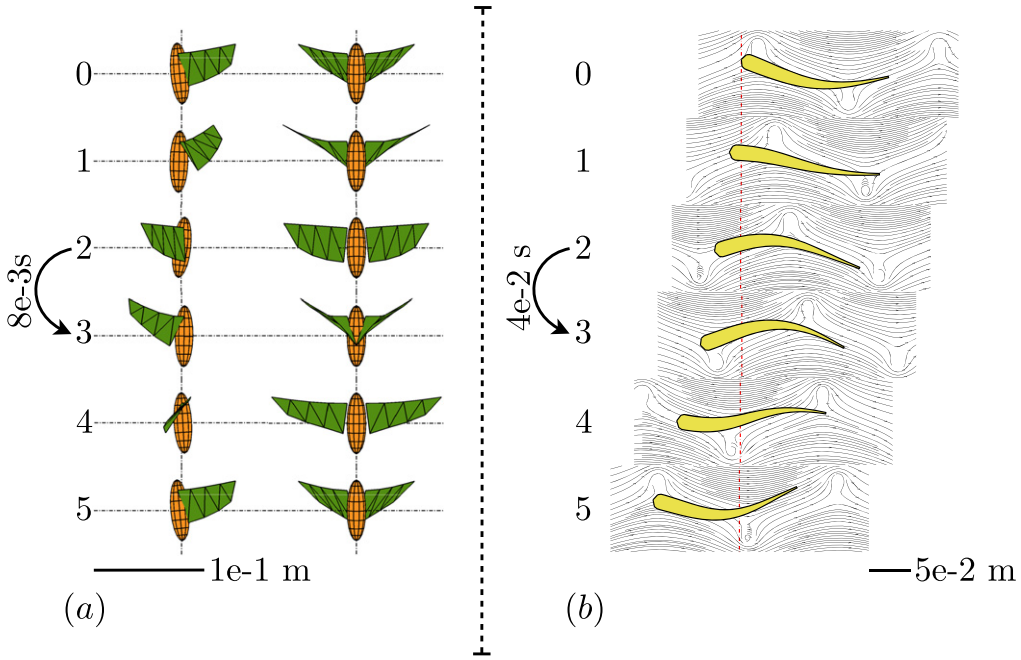

Figure 12. Soft locomotion: hovering flight (left) and passive swimming of a dead fish in a VKS (right). The wings and the fish body are modeled as passive Cosserat beams [17, 67] and simulated with the algorithm of figure 11.

approximated with the truncated basis of assumed modes [57]. Currently we are extending the Newton–Euler algorithms to the case of locomotive systems whose body deformations are described in the floating frame approach [15, 17]. All these algorithms are based on the following extension of the Newton–Euler model of discrete rigid systems derived in [16] for punctual joints:

$$\begin{pmatrix} \mathcal{M}_j & M_j^T \\ M_j & m_j \end{pmatrix}\begin{pmatrix} \dot{\eta}_j \\ \ddot{r}_{ej} \end{pmatrix} = \begin{pmatrix} \mathrm{ad}_{\eta_j}^T\left(\mathcal{M}_j\eta_j\right) + f_{\mathrm{ext}} \\ Q_j + Q_{\mathrm{ext}} \end{pmatrix}$$

$$+ \begin{pmatrix} f_j - \sum_{i/j=a(i)} Ad_{g_{i,j}}^T f_i \\ -\sum_{i/j=a(i)} \Phi_j^T R_{g_{j,i}} f_i \end{pmatrix}$$

$$g_j = g_i g_{ei} g_{aj},$$

$$\eta_j = Ad_{g_{j,i}}\eta_i + R_{g_{j,i}}\Phi_i\dot{r}_{ei} + A_j\dot{r}_j,$$

$$\dot{\eta}_j = Ad_{g_{j,i}}\dot{\eta}_i + R_{g_{j,i}}\Phi_i\ddot{r}_{ei} + \zeta_j.$$

Without entering into the details of this model, we note that it has as its configuration space $C = (SE(3) \times \mathbb{R}^{N_0})\times (SE(3) \times \mathbb{R}^{N_i}) \times ...(SE(3) \times \mathbb{R}^{N_{n_b}})$, where N_k is the

number of modal coordinates used to describe the deformation of the k^{th} body and n_b is the total number of joints. We also point out that the preceding model has the same form as its rigid version (29)–(32), where all the supplementary terms are introduced by the modal coordinates of the soft bodies brought together in the vectors of elastic coordinates r_{ej}. This model has been recently used to tackle constrained MMS dynamics with soft appendages [15].

10. Conclusion

In this article, we quickly reviewed several aspects of locomotion dynamics in bio-robotics. Starting from animals before moving on to real robots, we showed that there is a need to develop methodological tools for designing, modeling, control, and motion planning of a new generation of robots with many (external and internal) degrees of freedom. From this perspective, a basic Lagrangian picture of modeling using reduced velocities instead of momentum was presented. Particular attention was paid to the problem of the classification of systems. We discovered that behind their apparent diversity, many locomotion modes share common geometric structures. Although purely qualitative, this knowledge is useful for solving locomotion problems because it allows general solutions to be produced and is a desirable tool for guiding intuition and designing control laws. This classification endeavor was achieved from the perspective of solving a general basic problem of great interest in locomotion. This problem consists in computing the net motions (solution to the forward external dynamics) of an MMS as well as the internal torques (solution to the inverse internal dynamics) from knowledge of the evolution of internal joints. Although the Lagrangian approach offers a general synthetic point of view of a broad class of multibody systems, it is found wanting. In particular, when the number of internal degrees of freedom increases, Lagrangian models and their associated algorithms become increasingly heavy to handle, even numerically. For all these reasons, we presented recent results based on an alternative solution to the Lagrangian formulation that uses the well-known Newton–Euler formulation of robotics, which in the continuous case is coupled with the geometrically exact theory of Cosserat beams. This formulation leads to easily programmable and fast algorithms, which are capable of solving both forward external and inverse internal dynamics of discrete, continuous, and soft systems.

References

[1] www.youtube.com/watch?v=HfHRHoCBZCc
[2] http://euler.aero.iitb.ac.in/docs/MAV/www.darpa.mil/tto/MAV/mav auvsi.html
[3] www.avinc.com/nano.htm
[4] www.octopusproject.eu/results.html
[5] Abraham R and Marsden J E 1994 *Foundations of Mechanics* 2nd edn (Boulder, CO: Westview Press)
[6] Arnold V I 1966 Sur la geometrie differentielle des groupes de Lie de dimension infinie et ses applications a l'hydrodynamique des fluides parfaits *Ann. Inst. J. Fourier* **16** 319–61
[7] Arnold V I 1988 *Mathematical Methods in Classical Mechanics* (New York: Springer-Verlag)
[8] Arnold V I, Weinstein A and Vogtmann K 1989 *Mathematical Methods of Classical Mechanics* 2nd edn (New York: Springer)
[9] Beal D N, Hover F S, Triantafyllou M S, Liao J C and Lauder G V 2006 Passive propulsion in vortex wakes *J. Fluid Mech.* **549** 385–402
[10] Belkhiri A, Porez M and Boyer F 2012 A hybrid dynamic model of an insect-like mav with soft wings *ROBIO'2012: Proc. of IEEE Int. Conf. on Robotics and Biomimetics* 108–15
[11] Birkhoff G 1978 *Hydrodynamics: A Study in Logic Fact, and Similitude* (Westport, CT: Greenwood Press)
[12] Bloch A, Crouch P, Baillieul J and Marsden J 2007 *Nonholonomic Mechanics and Control* (New York: Springer-Verlag)
[13] Boyer F and Ali S 2011 Recursive inverse dynamics of mobile multibody systems with joints and wheels *IEEE Transactions on Robotics* **27** 215–28
[14] Boyer F, Ali S and Porez M 2012 Macro-continuous dynamics for hyper-redundant robots: application to kinematic locomotion bio-inspired by elongated body animals *IEEE Trans. Robot.* **28** 303–17
[15] Boyer F and Belkhiri A 2014 Reduced locomotion dynamics with passive internal dofs: application to nonholonomic and soft robotics *IEEE Trans. Robot.* **30** 578–92
[16] Boyer F and Coiffet P 1996 Generalization of Newton–Euler model for flexible manipulators *J. Robot. Syst.* **1** 11–24
[17] Boyer F, Porez M, Belkhiri A and Hunt A 2013 Locomotion dynamics for bio-inspired robots with soft appendages: application to hovering flight and passive swimming *IEEE Trans. Robot.* submitted
[18] Boyer F, Porez M and Khalil W 2006 Macro-continuous computed torque algorithm for a three-dimensional eel-like robot *IEEE Trans. Robot.* **22** 763–75
[19] Boyer F, Porez M and Leroyer A 2010 Poincaré–Cosserat equations for the Lighthill three-dimensional large amplitude elongated body theory: application to robotics *J. Nonlinear Sci.* **20** 47–79
[20] Boyer F and Primault D 2005 The Poincaré–Chetayev equations and flexible multibody systems *J. Appl. Math. Mech.* **69** 925–42
[21] Canavin J and Likins P 1977 Floating reference frames for flexible spacecraft *J. Spacecr. Rockets* **14** 724–32
[22] Candelier F, Boyer F and Leroyer A 2011 Three-dimensional extension of Lighthill's large-amplitude elongated-body theory of fish locomotion *J. Fluid Mech.* **674** 196–226
[23] Candelier F, Porez M and Boyer F 2013 Note on the swimming of an elongated body in a non-uniform flow *J. Fluid Mech.* **716** 616–37
[24] Cartan E 1946 *Lecons sur la géométrie des espaces de Riemann* 2nd edn (Paris: Gauthier-Villars)
[25] Chetayev N G 1927 *Sur les Équations de Poincaré* (Comptes rendus de l'Académie des Sciences de Paris)
[26] Chevallereau C and Aoustin Y 2001 Optimal reference trajectories for walking and running of a biped robot *Robotica* **19** 557–69
[27] Chevallereau C, Bessonnet G, Abba G and Aoustin Y 2009 *Bipedal Robots (CAM Control Systems, Robotics and Manufacturing Series)* (ISTE Wiley)
[28] Cianchetti M, Arienti A, Follador M, Mazzolai B, Dario P and Laschi C 2011 Design concept and validation of a robotic arm inspired by the octopus *Mater. Sci. Eng.* C **31** 1230–9
[29] Coquereaux R 2002 *Espaces Fibrés et Connexions* 3rd edn (Marseille: Centre de Physique Théorique de Luminy)
[30] Crespi A and Ijspeert A 2006 Amphibot II: an amphibious snake robot that crawls and swims using a central pattern generator *Proc. of the 9th Int. Conf. on Climbing and Walking Robots*

[31] Croon G D, Clercq K D, Ruijsink R and Remes B 2009 Design, aerodynamics, and vision-based control of the DelFly *Int. J. Micro Air Veh.* **1** 71–98
[32] Dickinson M H, Farley C T, Full R J, Koehl M A, Kram R and Lehman S 2000 How animals move: an integrative view *Science* **288** 100–6
[33] Dickinson M H, Lehmann F O and Sane S P 1999 Wing rotation and the aerodynamic basis of insect flight *Science* **284** 1954–60
[34] Ehresmann C 1950 *Les connexions infinitésimales dans un espace fibré différentiable* (Bruxelles: Colloque de Topologie) 29–55
[35] Frankel T 1998 *The Geometry of Physics: An Introduction* 2nd edn (Cambridge: Cambridge University Press)
[36] Goldstein H 2001 *Classical Mechanics* 3rd edn (Reading, MA: Addison Wesley)
[37] Gray J and Lissmann H W 1950 The kinetics of locomotion of the grass-snake *J. Exp. Biol.* **26** 354–67
[38] Grizzlek J W, Chevallereau C, Ames A and Sinnet R 2010 3D bipedal robotic walking: models, feedback control, and open problems nonlinear control systems *8th IFAC Symp. on Nonlinear Control Systems*
[39] Hannan M W and Walker I D 2001 Analysis and experiments with an elephant's trunk robot *Adv. Robot.* 847–58
[40] Hatton R L, Burton L J, Hosoi A E and Choset H 2011 Geometric maneuverability with applications to low Reynolds number swimming *Int. Conf. on Intelligent Robots and Systems* 3893–8
[41] Hatton R L and Choset H 2009 Generating gaits for snake robots by annealed chain fitting and keyframe wave extraction *IROS'09: Proc. IEEE/RSJ Int. Conf. Intell. Robots Syst.* 840–5
[42] Hatton R L and Choset H 2011 Geometric motion planning: The local connection, Stokes' theorem, and the importance of coordinate choice *Int. J. Robot. Res.* **30** 988–1014
[43] Hirose S 1993 *Biologically Inspired Robots: Snake-Like Locomotors and Manipulators* (Oxford: Oxford University Press)
[44] Horstmann J, Henningsson P, Thomas A L and Bomphrey R 2014 Wake development behind paired wings with tip and root trailing vortices: consequences for animal flight force estimates *PloS one* **9** e91,040
[45] Hu D L, Nirody J, Scott T and Shelley M J 2009 The mechanics of slithering locomotion *Proc. Nat. Acad. Sci.* **106** 10081–5
[46] Kanso E 2009 Swimming due to transverse shape deformations *J. Fluid Mech.* **631** 127–48
[47] Kanso E, Marsden J, Rowley C and Melli-Huber J 2005 Locomotion of articulated bodies in a perfect planar fluid *J. Nonlinear Sci.* **15** 255–89
[48] Kelly S D and Murray R M 1995 Geometric phases and robotic locomotion *J. Robot. Syst.* **12** 417–31
[49] Kelly S D and Murray R M 1996 The geometry and control of dissipative systems *Proc. 35th IEEE Conf. on Decision and Control* vol 1 981–6
[50] Khalil W, Gallot G and Boyer F 2007 Dynamic modeling and simulation of a 3-d serial eel like robot *IEEE Trans. Syst. Man Cybern.* C **37** 1259–68
[51] Kolomenskiy D, Casas J and Godoy-Diana R 2013 Large kinematic variability during take-off in butterflies due to varying relative timing of legs and aerodynamic forces *J. Exp. Biol.* **216** 3351–563
[52] Lamb H 1932 *Hydrodynamics* (Cambridge: Cambridge University Press)
[53] Liljeback P, Pettersen K Y, Stavdahl O and Gravdahl J T 2011 Experimental investigation of obstacle-aided locomotion with a snake robot *IEEE Trans. Robot.* **27** 792–800
[54] Liu H 2009 Integrated modeling of insect flight: from morphology, kinematics to aerodynamics *J. Comput. Phys.* **228** 439–59
[55] Marsden J E 1990 *Lectures on Mechanics* (*London Math. Society, Lecture Notes Ser.* vol 174) (Cambridge: Cambridge University Press)
[56] Marsden J E and Ratiu T S 1999 *Introduction to Mechanics and Symmetry* 2nd edn (New York: Springer-Verlag)
[57] Meirovitch L 1970 *Methods of Analytical Dynamics* (New York: McGraw-Hill)
[58] Melli J B, Rowley C W and Rufat D S 2006 Motion planning for an articulated body in a perfect planar fluid *SIAM J. Appl. Dyn. Syst.*
[59] Montgomery R 1993 *Gauge Theory of the Falling Cat in Dynamics and Control of Mechanical Systems* 1 ((American Mathematical Society)
[60] Muller U K, Heuvel B L E V D, Stamhuis E J and Videler J J 1997 Fish foot prints: morphology and energetics of the wake behind a continuously swimming mullet (chelon labrosus risso) *J. Exp. Biol.* **200** 2893–906
[61] Muller U K, Smit J, Stanhuis E J and Videler J J 2001 How the body contibutes to the wake in undulatory fish swimming: flow fields of a swimming eel (anguilla anguilla) *J. Exp. Biol.* **204** 2751–62
[62] Murray R M, Li Z and Sastry S S 1994 *Robotic Manipulation* (Boca Raton, FL: CRC Press)
[63] Ostrowski J 1999 Computing reduced equations for robotic systems with constraints and symmetries *IEEE Trans. Robot. Autom.* **15** 111–23
[64] Ostrowski J P and Burdick J W 1998 The geometric mechanics of undulatory robotics locomotion *Int. J. Robot. Res.* **17** 683–701
[65] Poincaré H 1901 Sur une forme nouvelle des équations de la mécanique *Compte Rendu de l'Académie des Sciences de Paris* **132** 369–71
[66] Poincaré H 1996 Œuvres. Tome VII. Masse fluides en rotation–Principes de mécanique analytique–Probléme des trois corps *Editions Jacques Gabay*
[67] Porez M, Boyer F and Belkhiri A 2013 A hybrid dynamic model for bio-inspired robots with soft appendages–application to a bio-inspired flexible flapping-wing micro air vehicle *ICRA'2014: IEEE Int. Conf. on Robotics and Automation* pp 1–8 submitted
[68] Porez M, Boyer F and Ijspeert A J 2014 Improved Lighthill fish swimming model for bio-inspired robots—modelling, computational aspects and experimental comparisons *Int. J. Robot. Res.* at press
[69] Purcell E M 1977 Life at low Reynolds number *Am. J. Phys.* **45** 3
[70] Reissner E 1973 On a one-dimensional large displacement finite-strain theory *Stud. Appl. Math.* **52** 87–95
[71] Richter C and Lipson H 2011 Untethered hovering flapping flight of a 3D-printed mechanical insect *Artificial Life* **17** 73–86
[72] Rumyantsev V V 1998 On the Poincaré and Chetayev equations *J. Appl. Math. Mech.* **62** 495–502
[73] Saunders F, Trimmer B A and Rife J 2011 Modeling locomotion of a soft-bodied arthropod using inverse dynamics *Bioinspir. Biomim.* **6** 016,001
[74] Shammas E, Choset H and Rizzi A 2005 Natural gait generation techniques for principally kinematic mechanical systems *Proc. Robotics: Science and Systems* (Cambridge, USA)
[75] Shapere A and Wilczek F 1989 Geometry of self-propulsion at low Reynolds number *J. Fluid Mech.* **198** 557–85
[76] Simo J C 1989 A finite strain beam formulation. The three-dimensional dynamic problem. Part I: formulation and optimal parametrization *Comp. Meth. Appl. Mech. Eng.* **72** 267–304
[77] Simo J C and Vu-Quoc L 1988 On the dynamics in space of rods undergoing large motions–a geometrically exact approach *Comput. Methods Appl. Mech. Eng.* **66** 125–61
[78] Spivak M 1999 *A Comprehensive Introduction to Differential Geometry* 3rd edn (Publish or Perish, INC.)
[79] Triantafyllou M S and Triantafyllou G S 1995 An efficient swimming machine *Sci. Am.* **272** 64–70
[80] Triantafyllou M S, Triantafyllou G S and Yue D K P 2000 Hydrodynamics of fishlike swimming *Ann. Rev. Fluid Mech.* **32** 33–53

[81] Wood R J 2007 Design, fabrication, and analysis of a 3DOF, 3cm flapping-wing MAV *IROS 2007: (Int. Conf. on Intelligent Robots and Systems 2007)* (IEEE/RSJ) 1576–81
[82] Wright C, Johnson A, Peck A, McCord Z, Naaktgeboren A, Gianfortoni P, Gonzalez-Rivero M, Hatton R and Choset H 2007 *Design of a Modular Snake Robot IEEE/RSJ Int. Conf. on Intelligent Robots and Systems* 2609–14
[83] Yamada H, Chigisaki S, Mori M, Takita K, Ogami K and Hirose S 2005 Development of amphibious snake-like robot ACM-R5 *Proc. 36th Int. Symp. on Robotics*

QUERY FORM

JOURNAL: Bioinspiration & Biomimetics

AUTHOR: F Boyer and M Porez

TITLE: Multibody system dynamics for bio-inspired locomotion: from geometric structures to computational aspects

ARTICLE ID: bb499053

No Query